

Isospin symmetry and analyticity in $D \rightarrow \bar{K}\pi\pi$ decays

Emi Kou^a, Tetiana Moskalets^b, and Bachir Moussallam^a

^aUniversité Paris-Saclay, Laboratoire de physique des 2 infinis Irène Joliot-Curie (CNRS/IN2P3,UMR9012), 91405 Orsay, France.

^bPhysikalisches Institut, Albert-Ludwigs-Universität Freiburg, Freiburg, Germany.

December 29, 2023

Abstract

We perform a detailed study of the consequences of isospin symmetry in the Cabibbo favoured $D \rightarrow \bar{K}\pi\pi$ decays. These processes are important for precision testing of the Standard Model and for hadronic physics. Combining isospin symmetry with a dispersive reconstruction theorem we derive a representation in terms of one-variable functions which allows one to predict all the $D \rightarrow \bar{K}\pi\pi$ amplitudes given inputs from one D^+ mode and one D^0 mode. From this, using dispersion relations and unitarity, we derive a set of 6+6 Khuri-Treiman type integral equations which enable to take three-body rescattering effects into account. A first test of this approach is presented using experimental results on the $D^+ \rightarrow K_S\pi^0\pi^+$ and the $D^0 \rightarrow K_S\pi^-\pi^+$ modes.

Contents

1	Introduction	2
2	Isospin decomposition of the $D \rightarrow \bar{K}\pi\pi$ amplitudes	5
2.1	Kinematics	5
2.2	Weak Hamiltonian	7
2.3	Isospin amplitudes and one-variable functions	8
2.4	Physical amplitudes in terms of $j = 0, 1$ one-variable functions	10

3	Unitarity, dispersion relations and Khuri-Treiman equations	12
3.1	Asymptotic behaviour and uniqueness conditions	12
3.2	Partial-waves and unitarity	13
3.3	Khuri-Treiman equations for the D^+ and D^0 functions	15
4	Solutions of the KT equations and fits to the data	17
4.1	πK and $\pi\pi$ phase-shifts and resonances	17
4.2	S -wave modelling in inelastic energy regions	19
4.3	Matrix approximations to the KT equations	20
4.4	D^+ fits	24
4.5	D^0 fits	28
4.6	Comparison of the F - and H -functions	34
5	Conclusions	35
A	Soft pion limits	37
B	Details of the expansions with isospin amplitudes	39
B.1	General relations	39
B.2	Crossing symmetries	41
C	Angular integrations	42
C.1	Hat-functions	42
C.2	Angular integrals expressed in terms of kernels	44
C.3	Breit-Wigner functions	48

1 Introduction

Precision measurements of non-leptonic weak decays of the K , D and B mesons provide crucial information on the origin of the violation of CP symmetry. In the last two decades, studies of CP violation in B decays by the Babar, Belle and LHCb collaborations have led to a considerable improvement in the precision of the determination of the three CKM angles α, β, γ (also called ϕ_1, ϕ_2, ϕ_3). This effort is due to be pursued at Belle II [1].

Non-leptonic decays of flavoured mesons probe dimension six operators as well as the dynamics of strong final-state rescattering. The D mesons differ from the K and the B ones in that, for the c quark, neither the light-quark nor the heavy-quark expansions can be justified. This difference could manifest itself in three-body decays. Indeed, final-state rescattering which involve the three particles are suppressed in K decays (they

vanish at LO and NLO in the chiral expansion¹) and are generally also suppressed in B decays within the QCD factorisation framework (see[5] and references therein). D decays, in contrast, could well be sensitive to three-body rescattering effects and it is still an open question whether such effects can be clearly identified in the data.

In this paper we reconsider the theoretical description of the family of three-body decays: $D^+, D^0 \rightarrow \bar{K}\pi\pi$. One motivation is related to the method proposed in refs. [6, 7, 8] (BPGGSZ) for measuring the angle γ (or ϕ_3), which is the most efficient one for that purpose. It uses the chain decay $B^\pm \rightarrow K^\pm D, D \rightarrow K_S \pi^- \pi^+$ and requires knowledge of the behaviour of both the strong phase and the modulus of the $D^0 \rightarrow K_S \pi^- \pi^+$ amplitude². While averages of these quantities can actually be measured (see below) a reliable modelling would further improve the accuracy of this approach. Another, different, motivation is provided by the experimental observation, some time ago, of several interesting features in the amplitude $D^+ \rightarrow K^- \pi^+ \pi^+$. Based on an isobar model description of the Dalitz plot, a first clear observation of the broad scalar κ resonance was reported by the E791 collaboration [10]. Moreover, this amplitude shows evidence of a significant dynamical role of *repulsive* interactions, as between a πK pair with $I = 3/2$ [11] (see also [12]) or a pion pair with isospin $I = 2$ [13], which are often ignored. Several theoretical models have been proposed for describing the $D^+ \rightarrow K^- \pi^+ \pi^+$ amplitude [14, 15, 16, 17, 18, 19, 20, 21].

We will combine two theoretical tools: isospin symmetry and dispersion relations. While not exact, of course, isospin symmetry is still a very precise dynamical constraint since isospin breaking effects are of the order $\sim 0.5 - 1\%$. Isospin decompositions of the four independent $K \rightarrow 3\pi$ amplitudes have been implemented a long time ago [22, 23]. Analogous application to the $D \rightarrow \bar{K}\pi\pi$ amplitudes could be performed as well, and is simplified by the fact that the relevant weak Hamiltonian, in that case, is a pure $I = 1$ operator. This was exploited previously in the work of Niecknig and Kubis [21, 24] who performed a combined study of the two modes $D^+ \rightarrow K^- \pi^+ \pi^+, \bar{K}^0 \pi^+ \pi^0$. They have also derived for the S - and the P -wave amplitudes a set of Khuri-Treiman (KT) dispersive equations [25, 26]. This formalism allows one to take three-body rescattering effects into account. The mode $D^+ \rightarrow K^- \pi^+ \pi^+$ has been studied in the analogous framework of Faddeev-type equations in refs. [19, 20].

We extend here the application of isospin symmetry and of the KT equations to *all* the three-body decay modes of the form $D \rightarrow \bar{K}\pi\pi$. That is, in addition to the two modes of the D^+ we will consider the three decay modes of the D^0 : $D^0 \rightarrow K^- \pi^+ \pi^0, \bar{K}^0 \pi^- \pi^+, \bar{K}^0 \pi^0 \pi^0$. The isospin relations which we provide are applicable, as well, to simpler models like the isobar model. The possibility of performing combined fits of several different amplitudes puts constraints on the theoretical models and could

¹The $K \rightarrow 3\pi$ amplitude at NLO has been computed in refs. [2, 3], the two-loop rescattering contributions have been evaluated in ref.[4].

²The same inputs can also be used in measurements of the $D^0 - \bar{D}^0$ mixing parameters [9].

also lead to a better determination of the small double-Cabibbo suppressed amplitudes which are present when a K_S (or a K_L) is detected in the final state. This would be useful in the search for a CP violating phase in this sector as proposed in ref. [27].

We perform a first test of our model using two sets of experimental data which we could access. The first set concerns measurements of the $D^+ \rightarrow K_S \pi^0 \pi^+$ mode performed by the BESIII collaboration [28]. Their results on the distribution of events are provided by the collaboration over a dense binning of the Dalitz plot (with 1342 bins). The second set of data refer to measurements by CLEO [29] and by BESIII [30] of the $D^0 \rightarrow K_S \pi^- \pi^+$ mode. The data, in this case, can be retrieved from tables in the publications. They are given on a limited number of bins (8 bins) but contain information both on the modulus squared of the amplitude and on its phase δ_D through averages \bar{c}_i, \bar{s}_i of the cosine and sine of the phase differences

$$\Delta\delta_D(s, u) \equiv \delta_D(s, t, u) - \delta_D(u, t, s) \quad (1.1)$$

(s, t, u being Mandelstam variables) performed over bin i . Remarkably, measuring such phases is possible in D^0 decays by making use of correlated D pairs, e.g from $\psi(3770) \rightarrow D^0 \bar{D}^0$, and tagging one of the D 's in a CP even/odd state [7, 31].

The plan of the paper is as follows. After introducing some notation and reviewing the structure of the relevant weak Hamiltonian we implement the Wigner-Eckart theorem on a number of $2 \rightarrow 2$ matrix elements. A rather predictive structure emerges when this is combined with the dispersive “reconstruction theorem” [25, 32, 33] which we first limit to $j = 0, 1$ partial-waves. The two D^+ decay amplitudes get expressed in terms of six functions of one variable (the F -functions), as was found in [21, 24]. The new results concern the D^0 amplitudes for which we provide expressions involving the same F -functions plus an additional set of six functions (the H -functions).

Using these results two sets of KT integral equations are derived, from which the F - and the H -functions can be computed numerically, depending in a linear way respectively on 6 and on 6+7 complex polynomial parameters. These form the core of our model for describing the amplitudes in the whole Dalitz plot region. The determination of the parameters based on the input experimental data mentioned above is then discussed. In addition, we use qualitative information which derives from four independent soft pion theorems and we consider the decay widths of the five $D \rightarrow \bar{K} \pi \pi$ modes. These widths are very different from each other and provide good probes of the interference patterns between the isospin F - and H -functions. We finally comment on the difference between the F and the H I=1/2 S -waves near the πK threshold.

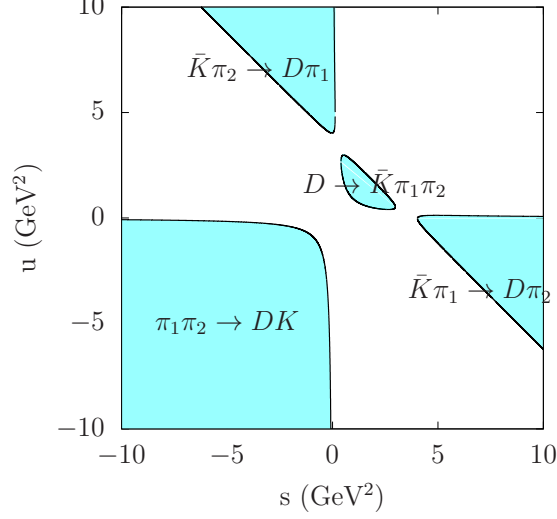


Figure 1: Physical regions for decay and for scattering as a function of the variables u , s .

2 Isospin decomposition of the $D \rightarrow \bar{K} \pi \pi$ amplitudes

2.1 Kinematics

We consider amplitudes $D(p_D) \rightarrow \bar{K}(p_K)\pi_1(p_{\pi_1})\pi_2(p_{\pi_2})$. The Mandelstam variables s , u , t are defined as follows

$$s = (p_K + p_{\pi_1})^2, \quad u = (p_K + p_{\pi_2})^2, \quad t = (p_{\pi_1} + p_{\pi_2})^2. \quad (2.1)$$

and satisfy

$$s + t + u = \Sigma, \quad \Sigma = m_D^2 + m_K^2 + 2m_\pi^2. \quad (2.2)$$

The decay amplitudes are called $\mathcal{A}_{\bar{K}\pi_1\pi_2}(s, t, u)$ and the differential decay width is given by

$$\frac{d^2\Gamma_{\bar{K}\pi_1\pi_2}}{dsdt} = \frac{1}{256\pi^3 m_D^3} |\mathcal{A}_{\bar{K}\pi_1\pi_2}(s, t, u)|^2. \quad (2.3)$$

A symmetry factor $S_{12} = 1/2$ must be appended when integrating over t when the two pions are identical. By analytical continuation, the amplitude functions $\mathcal{A}_{\bar{K}\pi_1\pi_2}(s, t, u)$ also describe scattering processes, the physical regions are shown in fig. 1. Next, we recall the definitions of the angular variables θ_s and θ_t associated with the $\bar{K}\pi_1$ and $\pi_1\pi_2$ reference frames.

1) $\bar{K}\pi_1$ CMS

We first consider the $\bar{K}\pi_1$ centre-of-mass system (fig. 2, left). The 4-momenta in this

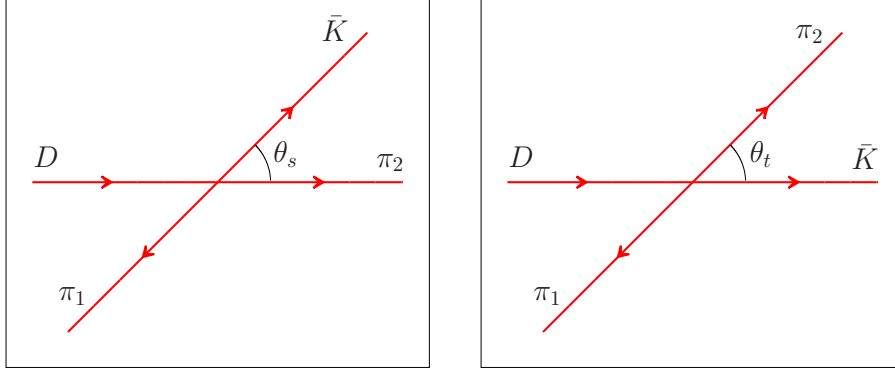


Figure 2: Kinematics of $D \rightarrow \bar{K}\pi_1\pi_2$ in the $\bar{K}\pi_1$ (left) and the $\pi_1\pi_2$ centre-of-mass systems showing the definitions of the angles θ_s and θ_t .

frame read

$$p_D = \frac{1}{2\sqrt{s}} \begin{pmatrix} s + \Delta_{D\pi} \\ \lambda_{D\pi}^{1/2}(s) \hat{u} \end{pmatrix}, \quad p_{\pi_2} = \frac{1}{2\sqrt{s}} \begin{pmatrix} \Delta_{D\pi} - s \\ \lambda_{D\pi}^{1/2}(s) \hat{u} \end{pmatrix} \quad (2.4)$$

and

$$p_K = \frac{1}{2\sqrt{s}} \begin{pmatrix} s + \Delta_{K\pi} \\ \lambda_{K\pi}^{1/2}(s) \hat{v} \end{pmatrix}, \quad p_{\pi_1} = \frac{1}{2\sqrt{s}} \begin{pmatrix} s - \Delta_{K\pi} \\ -\lambda_{K\pi}^{1/2}(s) \hat{v} \end{pmatrix} \quad (2.5)$$

with the definitions

$$\Delta_{AB} = m_A^2 - m_B^2, \quad \lambda_{AB}(s) = (s - (m_A + m_B)^2)(s - (m_A - m_B)^2). \quad (2.6)$$

In eq. (2.5) \hat{u} and \hat{v} are unit 3-vectors and we define the cosine of the scattering angle in this frame as

$$z_s \equiv \cos(\theta_s) = \hat{u} \cdot \hat{v} = \frac{s(t - u) + \Delta_{D\pi}\Delta_{K\pi}}{\sqrt{\lambda_{D\pi}(s)\lambda_{K\pi}(s)}}. \quad (2.7)$$

From this, t and u can be written in terms of s and z_s as,

$$\begin{aligned} t(s, z_s) &= \frac{1}{2} \left(\Sigma - s - \frac{\Delta}{s} + \kappa_s(s) z_s \right) \\ u(s, z_s) &= \frac{1}{2} \left(\Sigma - s + \frac{\Delta}{s} - \kappa_s(s) z_s \right) \end{aligned} \quad (2.8)$$

with

$$\Delta = \Delta_{D\pi}\Delta_{K\pi}, \quad \kappa_s(s) = \frac{\sqrt{\lambda_{D\pi}(s)\lambda_{K\pi}(s)}}{s}. \quad (2.9)$$

2) $\pi_1\pi_2$ CMS:

In the $\pi_1\pi_2$ centre-of-mass system (fig. 2, right) the momenta read

$$p_D = \frac{1}{2\sqrt{t}} \begin{pmatrix} t + \Delta_{DK} \\ \lambda_{DK}^{1/2}(t)\hat{u} \end{pmatrix}, \quad p_K = \frac{1}{2\sqrt{t}} \begin{pmatrix} \Delta_{DK} - t \\ \lambda_{DK}^{1/2}(t)\hat{u} \end{pmatrix} \quad (2.10)$$

and

$$p_{\pi_1} = \frac{1}{2\sqrt{t}} \begin{pmatrix} t \\ -\lambda_{\pi\pi}^{1/2}(t)\hat{v} \end{pmatrix}, \quad p_{\pi_2} = \frac{1}{2\sqrt{t}} \begin{pmatrix} t \\ \lambda_{\pi\pi}^{1/2}(t)\hat{v} \end{pmatrix}. \quad (2.11)$$

The cosine of the scattering angle z_t in this frame is then given by

$$z_t(s, t, u) \equiv \cos(\theta_t) = \frac{s - u}{\sqrt{\lambda_{DK^0}(t) (1 - 4m_\pi^2/t)}} \quad (2.12)$$

and one can express s and u in terms of t and z_t

$$\begin{aligned} s(t, z_t) &= \frac{1}{2} (\Sigma - t + \kappa_t(t) z_t) \\ u(t, z_t) &= \frac{1}{2} (\Sigma - t - \kappa_t(t) z_t) \end{aligned} \quad (2.13)$$

with

$$\kappa_t(t) = \sqrt{\lambda_{DK}(t)(1 - 4m_\pi^2/t)}. \quad (2.14)$$

2.2 Weak Hamiltonian

In the Standard Model the $D \rightarrow \bar{K}\pi\pi$ decays are driven by the following weak Hamiltonian

$$H_W^{(CF)} = \frac{G_F}{\sqrt{2}} [V_{cs}^* V_{ud} (C_1 O_1 + C_2 O_2) + h.c.] \quad (2.15)$$

with

$$O_1 = (\bar{s}_i c_j)_{V-A} (\bar{u}_j d_i)_{V-A}, \quad O_2 = (\bar{s}_i c_i)_{V-A} (\bar{u}_j d_j)_{V-A} \quad (2.16)$$

(e.g. ref. [34]). It is Cabibbo favoured, i.e. $O(\lambda^0)$ in the Wolfenstein parametrisation [35], with [36]

$$|V_{cs}^* V_{ud}| = 0.969 \pm 0.016. \quad (2.17)$$

An important property, as can be seen immediately from (2.16) is that the $H_W^{(CF)}$ transforms under isospin as an $I = 1$ operator

$$H_W^{(CF)} \sim T_{II_z}, \quad I = 1, I_z = -1 \quad (2.18)$$

which will enable us to make use of the Wigner-Eckart theorem (e.g. [37])

$$\langle I_1 m_1 | T_{I, I_z} | I_2 m_2 \rangle = \langle II_z; I_2 m_2 | I_1 m_1 \rangle \mathcal{F}_I^{I_1 I_2} \quad (2.19)$$

when evaluating matrix elements.

In experimental situations where $K_S\pi_1\pi_2$ or $K_L\pi_1\pi_2$ are detected, contributions from $D \rightarrow K\pi_1\pi_2$ amplitudes must be considered, which are driven by the Hamiltonian

$$H_W^{(DCS)} = \frac{G_F}{\sqrt{2}} \left[V_{us}^* V_{cd} \left(C_1 \tilde{O}_1 + C_2 \tilde{O}_2 \right) + h.c. \right] \quad (2.20)$$

where

$$\tilde{O}_1 = (\bar{d}_i c_j)_{V-A} (\bar{u}_j s_i)_{V-A}, \quad \tilde{O}_2 = (\bar{d}_i c_i)_{V-A} (\bar{u}_j s_j)_{V-A}. \quad (2.21)$$

$H_W^{(DCS)}$ is doubly Cabibbo suppressed, i.e. $O(\lambda^2)$, with

$$|V_{us}^* V_{cd}| = 0.049 \pm 0.001. \quad (2.22)$$

From the point of view of isospin, it has both an $I = 0$ and a $I = 1$ component

$$H_W^{(DCS)} \sim \frac{1}{\sqrt{2}} T_{00} + \frac{1}{\sqrt{2}} T_{10}. \quad (2.23)$$

In that situation, isospin symmetry is less predictive than in the case of the Cabibbo favoured operator. Performing an expansion of the DCS amplitudes in terms of isospin one-variable functions analogous to the ones presented below in eqs. (2.33) to (2.37) for the CF amplitudes would involve 18 such functions instead of 12.

2.3 Isospin amplitudes and one-variable functions

It proves convenient to think in terms of scattering, rather than decay, amplitudes i.e. to consider the processes

$$\bar{K}\pi_1 \rightarrow D\pi_2, \quad \bar{K}\pi_2 \rightarrow D\pi_1, \quad \pi_1\pi_2 \rightarrow DK \quad (2.24)$$

which are associated with the matrix elements $\langle D\pi_i | H_W | \bar{K}\pi_j \rangle$ and $\langle DK | H_W | \pi_1\pi_2 \rangle$ (dropping the CF index). The first ones will be expressed in terms of isospin amplitudes labelled with a pair of half-integer isospins, referring to the initial and final state, and the latter ones will be labelled with a pair of integer isospins

$$\begin{aligned} \langle D\pi_i | H_W | \bar{K}\pi_j \rangle &: \mathcal{F}^{\frac{3}{2}\frac{3}{2}}(s, t, u), \mathcal{F}^{\frac{1}{2}\frac{3}{2}}(s, t, u), \mathcal{F}^{\frac{3}{2}\frac{1}{2}}(s, t, u), \mathcal{F}^{\frac{1}{2}\frac{1}{2}}(s, t, u) \\ \langle DK | H_W | \pi_1\pi_2 \rangle &: \mathcal{G}^{10}(s, t, u), \mathcal{G}^{12}(s, t, u), \mathcal{G}^{01}(s, t, u), \mathcal{G}^{11}(s, t, u). \end{aligned} \quad (2.25)$$

The explicit relations between the physical matrix elements and the isospin amplitudes are derived in a straightforward way by applying the Wigner-Eckart theorem (2.19): they are given in table 4 in appendix B. Using these, one can derive four relations among the five physical D decay amplitudes (e.g. [38, 39]). The first one relates the two D^+ amplitudes

$$\mathcal{A}_{K^-\pi^+\pi^+}(s, t, u) = -\sqrt{2}(\mathcal{A}_{\bar{K}^0\pi^0\pi^+}(s, t, u) + \mathcal{A}_{\bar{K}^0\pi^0\pi^+}(u, t, s)) \quad (2.26)$$

and the next two relations involve D^+ and D^0 amplitudes and are symmetric under s , u interchange

$$\begin{aligned}\mathcal{A}_{K^-\pi^+\pi^+}(s, t, u) &= \sqrt{2}(\mathcal{A}_{K^-\pi^0\pi^+}(s, t, u) + \mathcal{A}_{K^-\pi^0\pi^+}(u, t, s)) \\ \mathcal{A}_{K^-\pi^+\pi^+}(s, t, u) &= \mathcal{A}_{\bar{K}^0\pi^-\pi^+}(s, t, u) + \mathcal{A}_{\bar{K}^0\pi^-\pi^+}(u, t, s) - 2\mathcal{A}_{\bar{K}^0\pi^0\pi^0}(s, t, u)\end{aligned}\quad (2.27)$$

while the last relation involves antisymmetrised amplitudes

$$\begin{aligned}\mathcal{A}_{\bar{K}^0\pi^0\pi^+}(s, t, u) - \mathcal{A}_{\bar{K}^0\pi^0\pi^+}(u, t, s) &= \mathcal{A}_{K^-\pi^0\pi^+}(s, t, u) - \mathcal{A}_{K^-\pi^0\pi^+}(u, t, s) \\ &\quad - \sqrt{2}(\mathcal{A}_{\bar{K}^0\pi^-\pi^+}(s, t, u) - \mathcal{A}_{\bar{K}^0\pi^-\pi^+}(u, t, s)).\end{aligned}\quad (2.28)$$

In order to go beyond these general results it is convenient, at first, to make use of a redefined set of isospin amplitudes which leads to simpler expressions for the D^+ amplitudes: this is explained in appendix B. This set is labelled with the isospins of the $\bar{K}\pi$ or $\pi\pi$ systems only as it mixes the isospins of the $D\pi$ or DK states and we collect them into vectors $\vec{\mathcal{F}}(s, t, u)$ and $\vec{\mathcal{G}}(s, t, u)$

$$\vec{\mathcal{F}}(s, t, u) \equiv \begin{pmatrix} \mathcal{F}^{3/2}(s, t, u) \\ \mathcal{F}^{1/2}(s, t, u) \\ \mathcal{H}^{3/2}(s, t, u) \\ \mathcal{H}^{1/2}(s, t, u) \end{pmatrix}, \quad \vec{\mathcal{G}}(s, t, u) \equiv \begin{pmatrix} \mathcal{G}^0(s, t, u) \\ \mathcal{G}^2(s, t, u) \\ \mathcal{G}^1(s, t, u) \\ \tilde{\mathcal{G}}^1(s, t, u) \end{pmatrix}\quad (2.29)$$

These vectors satisfy the following crossing symmetry relations

$$\vec{\mathcal{G}}(t, s, u) = \mathbf{C}_{st}\vec{\mathcal{F}}(s, t, u), \quad \vec{\mathcal{F}}(u, t, s) = \mathbf{C}_{us}\vec{\mathcal{F}}(s, t, u), \quad (2.30)$$

the matrices \mathbf{C}_{st} , \mathbf{C}_{us} are given in eq. (B.9) in appendix B.2. We next use an approximation in which these isospin amplitudes are written as a finite sum of terms involving a function of one of the Mandelstam variables times an angular factor. This structure can be derived from dispersion theory, upon truncating the partial-wave expansion in the absorptive parts to $j = 0, 1$ [25, 32, 33]. The derivation shows that the one-variable functions which are involved are analytic with a right-hand cut. It has been adapted to the $D \rightarrow \bar{K}\pi\pi$ amplitudes (also including $j = 2$) in ref. [40]. We will assume here that the contributions generated by the $j \geq 2$ partial-waves in the absorptive parts can be approximated by an isobar-type model. The relevance of this description for $D \rightarrow \bar{K}\pi\pi$ is motivated by the experimental observation of a large dominance of the S and P waves in the Dalitz plot region. Restricting to $j = 0, 1$ for the moment, there are twelve one-variable functions which are involved: F_j^K , H_j^K , G_0^I , G_1^I , \tilde{G}_1^I . Collecting them into vectors as follows

$$\vec{F}_0(z) = \begin{pmatrix} F_0^{3/2}(z) \\ F_0^{1/2}(z) \\ H_0^{3/2}(z) \\ H_0^{1/2}(z) \end{pmatrix}, \quad \vec{F}_1(z) = \begin{pmatrix} F_1^{3/2}(z) \\ F_1^{1/2}(z) \\ H_1^{3/2}(z) \\ H_1^{1/2}(z) \end{pmatrix}, \quad \vec{G}_0(z) = \begin{pmatrix} G_0^0(z) \\ G_0^2(z) \\ 0 \\ 0 \end{pmatrix}, \quad \vec{G}_1(z) = \begin{pmatrix} 0 \\ 0 \\ G_1^1(z) \\ \tilde{G}_1^1(z) \end{pmatrix}\quad (2.31)$$

and taking into account the crossing relations (2.30), one easily arrives at the following representations for the $D \rightarrow \bar{K} \pi \pi$ isospin amplitudes $\vec{\mathcal{F}}$ and $\vec{\mathcal{G}}$

$$\begin{aligned}
\vec{\mathcal{F}}(s, t, u) &= \vec{F}_0(s) + (s(t-u) + \Delta)\vec{F}_1(s) + \mathbf{C}_{us}[\vec{F}_0(u) + (u(t-s) + \Delta)\vec{F}_1(u)] \\
&\quad + \mathbf{C}_{st}^{-1}[\vec{G}_0(t) + (s-u)\vec{G}_1(t)] \\
\vec{\mathcal{G}}(t, s, u) &= \vec{G}_0(t) + (s-u)\vec{G}_1(t) + \mathbf{C}_{st}[\vec{F}_0(s) + (s(t-u) + \Delta)\vec{F}_1(s)] \\
&\quad + \mathbf{C}_{st}\mathbf{C}_{us}[\vec{F}_0(u) + (u(t-s) + \Delta)\vec{F}_1(u)] .
\end{aligned} \tag{2.32}$$

2.4 Physical amplitudes in terms of $j = 0, 1$ one-variable functions

Using eqs. (2.32), (2.31) together with table 5 in appendix B one can express the physical amplitudes in terms of the twelve one-variable isospin functions introduced above. The D^+ amplitudes involve only six of them: $F_0^{1/2}$, $F_0^{3/2}$, $F_1^{1/2}$, $F_1^{3/2}$, G_0^2 and G_1^1 (called collectively the F -functions). The D^0 amplitudes involve the same six F -functions plus six additional ones: $H_0^{1/2}$, $H_0^{3/2}$, $H_1^{1/2}$, $H_1^{3/2}$, G_0^0 and \tilde{G}_1^1 (called H -functions in the following). The expressions of all the physical amplitudes are listed below, starting with the D^+ amplitudes.

1- D^+ amplitudes:

The two amplitudes $D^+ \rightarrow K^- \pi^+ \pi^+$ and $D^+ \rightarrow \bar{K}^0 \pi^0 \pi^+$ have the following expressions

$$\begin{aligned}
\mathcal{A}_{K^- \pi^+ \pi^+}(s, t, u) &= -\sqrt{2} \left[F_0^{3/2}(s) + F_0^{1/2}(s) + Z_s(F_1^{3/2}(s) + F_1^{1/2}(s)) \right. \\
&\quad \left. + (s \leftrightarrow u) \right] + G_0^2(t) \\
\mathcal{A}_{\bar{K}^0 \pi^0 \pi^+}(s, t, u) &= -2F_0^{3/2}(s) + F_0^{1/2}(s) + Z_s(-2F_1^{3/2}(s) + F_1^{1/2}(s)) \\
&\quad + 3F_0^{3/2}(u) + 3Z_u F_1^{3/2}(u) - \frac{\sqrt{2}}{4}G_0^2(t) + (s-u)G_1^1(t)
\end{aligned} \tag{2.33}$$

where

$$Z_s = s(t-u) + \Delta, \quad Z_u = u(t-s) + \Delta \tag{2.34}$$

are the $j = 1$ angular factors. The above formulae are in agreement with the result of ref. [21]³.

³The functions used here are proportional to those of ref. [21]: $F_j^{3/2} = (-1)^j \mathcal{F}_j^{3/2} / \sqrt{15}$, $F_j^{1/2} = (-1)^{j+1} \mathcal{F}_j^{1/2} / \sqrt{6}$, $G_0^2 = \mathcal{F}_0^2$, $G_1^1 = \mathcal{F}_1^1 \sqrt{3/8}$.

2) D^0 amplitudes:

The $D^0 \rightarrow K^- \pi^0 \pi^+$ amplitude reads

$$\begin{aligned}
\mathcal{A}_{K^- \pi^0 \pi^+}(s, t, u) = & -2 F_0^{3/2}(s) + F_0^{3/2}(u) - F_0^{1/2}(u) \\
& -2 Z_s F_1^{3/2}(s) + Z_u (F_1^{3/2}(u) - F_1^{1/2}(u)) \\
& + \frac{\sqrt{2}}{4} G_0^2(t) + (s - u) G_1^1(t) \\
& + \sqrt{2} \left(H_0^{3/2}(s) - H_0^{3/2}(u) + Z_s H_1^{3/2}(s) - Z_u H_1^{3/2}(u) \right) \\
& - \frac{\sqrt{2}}{2} \left(H_0^{1/2}(s) - H_0^{1/2}(u) + Z_s H_1^{1/2}(s) - Z_u H_1^{1/2}(u) \right) \\
& - 2(s - u) \tilde{G}_1^1(t) .
\end{aligned} \tag{2.35}$$

The contributions from the H -functions in this amplitude are antisymmetric under s, u interchange, they cancel when the amplitude is symmetrised in s, u , which is expected from the first isospin symmetry relation in eq. (2.27).

The $D^0 \rightarrow \bar{K}^0 \pi^- \pi^+$ amplitude reads

$$\begin{aligned}
\mathcal{A}_{\bar{K}^0 \pi^- \pi^+}(s, t, u) = & \sqrt{2} \left(F_0^{3/2}(s) + Z_s F_1^{3/2}(s) \right) + \frac{1}{6} G_0^2(t) \\
& - \left(H_0^{3/2}(s) + H_0^{1/2}(s) + Z_s (H_1^{3/2}(s) + H_1^{1/2}(s)) \right) \\
& - 3 \left(H_0^{3/2}(u) + Z_u H_1^{3/2}(u) \right) - G_0^0(t) - \sqrt{2} (s - u) \tilde{G}_1^1(t) .
\end{aligned} \tag{2.36}$$

Finally, the $D^0 \rightarrow \bar{K}^0 \pi^0 \pi^0$ amplitude's expression is

$$\begin{aligned}
\mathcal{A}_{\bar{K}^0 \pi^0 \pi^0}(s, t, u) = & \sqrt{2} \left[F_0^{3/2}(s) + \frac{1}{2} F_0^{1/2}(s) + Z_s (F_1^{3/2}(s) + \frac{1}{2} F_1^{1/2}(s)) + (s \leftrightarrow u) \right] \\
& - \frac{1}{3} G_0^2(t) - \left[2 H_0^{3/2}(s) + \frac{1}{2} H_0^{1/2}(s) + Z_s (2 H_1^{3/2}(s) + \frac{1}{2} H_1^{1/2}(s)) \right. \\
& \left. + (s \leftrightarrow u) \right] - G_0^0(t) .
\end{aligned} \tag{2.37}$$

We discuss below how to derive the functions F_j^K, H_j^K, G_j^I with $j = 0, 1$ from a set of Khuri-Treiman equations. The formulas above can be used, if one wishes, within simpler isobar model approaches. In order to properly describe the physical amplitudes it proves necessary to introduce some $j = 2$ contributions. It is not difficult to extend the above formulas to include $j = 2$ resonances consistently with isospin symmetry. One must simply perform the following replacements,

$$\begin{aligned}
Z_w F_1^K(w) & \rightarrow Z_w F_1^K(w) + Z_{2w} F_2^K(w) \\
Z_w H_1^K(w) & \rightarrow Z_w H_1^K(w) + Z_{2w} H_2^K(w) \\
G_0^0(t) & \rightarrow G_0^0(t) + Z_{2t} G_2^0(t)
\end{aligned} \tag{2.38}$$

where $w = s, u$ and one can take for the $j = 2$ angular functions

$$\begin{aligned}
Z_{2w} & = 3Z_s^2 - \lambda_{D\pi}(w) \lambda_{K\pi}(w) \\
Z_{2t} & = 3t(s - u)^2 - \lambda_{DK}(t)(t - 4m_\pi^2) .
\end{aligned} \tag{2.39}$$

3 Unitarity, dispersion relations and Khuri-Treiman equations

In this section we formulate a set of Khuri-Treiman type equations for the isospin one-variable functions. Let us first consider the asymptotic behaviour of the amplitudes, which conditions the number of subtractions needed in their dispersive representations.

3.1 Asymptotic behaviour and uniqueness conditions

Letting the variable s go to infinity while keeping t fixed and small the leading asymptotic behaviour of the isospin amplitudes $\mathcal{H}^{1/2}$, $\mathcal{H}^{3/2}$ is given by Pomeron exchange, while the behaviour of the amplitudes $\mathcal{F}^{1/2}$, $\mathcal{F}^{3/2}$ is given by the ρ Reggeon exchange. Therefore, a dispersion relation in the variable s for the amplitudes \mathcal{H}^I requires two subtractions while a single subtraction is needed in the case of \mathcal{F}^I . Now, when t goes to infinity and the variable s is kept fixed, the asymptotic behaviour is given by the K^* , K_2^* Reggeon exchanges. A dispersion relation in t thus requires one subtraction.

Here, in order to improve the description in the finite energy region of interest, we use a number of subtractions larger than the minimal one and assume twice-subtracted dispersion relations for all amplitudes. This assumption, which must be considered as part of the model, leads to the following asymptotic behaviour

$$\begin{aligned} \lim_{s \rightarrow \infty} \mathcal{A}_i(s, t, u) \Big|_{t \text{ fixed}} &\sim s \\ \lim_{t \rightarrow \infty} \mathcal{A}_i(s, t, u) \Big|_{s \text{ fixed}} &\sim t . \end{aligned} \tag{3.1}$$

The corresponding asymptotic behaviour of the one-variable functions is then as follows

$$\begin{aligned} F_0^{1/2}(s), F_0^{3/2}, H_0^{1/2}(s), H_0^{3/2} &\sim s \\ F_1^{1/2}(s), F_1^{3/2}, H_1^{1/2}(s), H_1^{3/2} &\sim s^{-1} \\ G_0^2(t), G_0^0(t) &\sim t \\ G_1^1(t), \tilde{G}_1^1(t) &\sim t^0 . \end{aligned} \tag{3.2}$$

Because there are only two independent Mandelstam variables, there is a family of re-definitions of the one-variable functions which leave the physical amplitudes invariant [32]. Using the vectorial notation (2.31) linear translations consistent with the asymptotic behaviour are as follows

$$\begin{aligned} \vec{F}_0(z) &\rightarrow \vec{F}_0(z) + \vec{a}_0 + \vec{b}_0 z \\ \vec{G}_0(z) &\rightarrow \vec{G}_0(z) + \vec{a}_{0G} + \vec{b}_{0G} z \\ \vec{G}_1(z) &\rightarrow \vec{G}_1(z) + \vec{a}_{1G} \end{aligned} \tag{3.3}$$

where the vectors \vec{a}_{0G} , \vec{b}_{0G} , \vec{a}_{1G} have two vanishing components. Inserting this into eq. (2.32) for the full amplitude it is easy to verify, using eq. (2.2), that it is left invariant

under the family of translations (3.3) in which the 14 parameters satisfy the conditions

$$\begin{aligned}
\vec{a}_{0G} + \text{diag}(1, 1, 0, 0)\mathbf{C}_{st}(2\vec{a}_0 + \Sigma\vec{b}_0) &= 0 \\
\vec{b}_{0G} - \text{diag}(1, 1, 0, 0)\mathbf{C}_{st}\vec{b}_0 &= 0 \\
\vec{a}_{1G} + \text{diag}(0, 0, 1, 1)\mathbf{C}_{st}\vec{b}_0 &= 0
\end{aligned} \tag{3.4}$$

such that 8 parameters can be chosen arbitrarily. In order to define uniquely the one-variable functions we must therefore impose eight conditions. In the following, we will set

$$\begin{aligned}
F_0^{3/2}(0) = \dot{F}_0^{3/2}(0) = H_0^{3/2}(0) = \dot{H}_0^{3/2}(0) &= 0 \\
G_0^2(0) = \dot{G}_0^2(0) = G_0^0(0) = \dot{G}_0^0(0) &= 0 .
\end{aligned} \tag{3.5}$$

3.2 Partial-waves and unitarity

The one-variable functions introduced above satisfy dispersion representations as a function of their discontinuities across the right-hand cuts (see eqs. (C.8), (C.10) in appendix C.2). These discontinuities can be derived from unitarity relations of $2 \rightarrow 2$ partial-wave amplitudes [25]. In our case, these amplitudes are $\bar{K}\pi \rightarrow D\pi$ (s -channel) and $\pi\pi \rightarrow DK$ (t -channel). We define the partial-waves in the s -channel as

$$\vec{\mathcal{F}}_j(s) = \frac{2j+1}{2} \frac{1}{(s\kappa_s(s))^j} \int_{-1}^1 dz_s P_j(z_s) \vec{\mathcal{F}}(s, t, u) \tag{3.6}$$

where P_j is a Legendre polynomial. In the integrand of eq. (3.6), we have to express t , u in terms of s , z_s as given in eq. (2.8). Similarly, in the t -channel, the partial-waves are defined as

$$\vec{\mathcal{G}}_j(t) = \frac{2j+1}{2} \frac{1}{(\kappa_t(t))^j} \int_{-1}^1 dz_t P_j(z_t) \vec{\mathcal{G}}(t, s, u) \tag{3.7}$$

and the variables s , u in the integrand must be expressed in terms of t and z_t using eq. (2.13).

Inserting the representation (2.32) of the amplitudes $\vec{\mathcal{F}}(s, t, u)$ and $\vec{\mathcal{G}}(t, s, u)$ in terms of single-variable functions into the angular integrals (3.6), (3.7), the s -channel $j = 0, 1$ partial-waves get expressed as a sum of two functions

$$\begin{aligned}
\mathcal{F}_0^K(s) &= F_0^K(s) + \widehat{F}_0^K(s) \\
\mathcal{H}_0^K(s) &= H_0^K(s) + \widehat{H}_0^K(s) \\
\mathcal{F}_1^K(s) &= F_1^K(s) + \widehat{F}_1^K(s) \\
\mathcal{H}_1^K(s) &= H_1^K(s) + \widehat{H}_1^K(s)
\end{aligned} \tag{3.8}$$

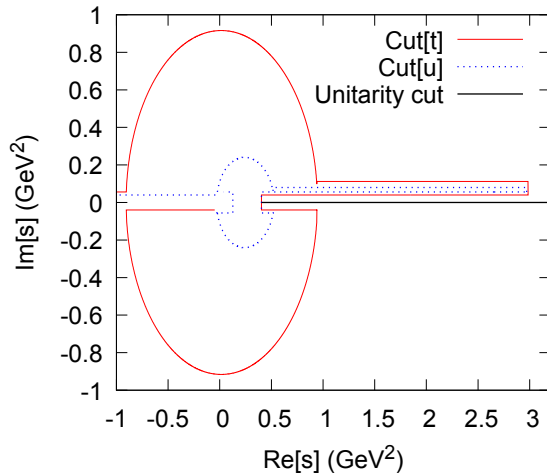


Figure 3: Complex cuts of the hat-functions $\hat{F}_j^K(s)$, $\hat{H}_j^K(s)$ illustrating the $m_D^2 + i\epsilon$ prescription. The solid red curve is generated from the z_s angular integrations of the functions of t and the blue dotted curve is generated from the integrations of the functions of u . The thick black line is the unitarity cut.

and the $j = 0, 1$ partial-waves in the t -channel have a similar form,

$$\begin{aligned}
\mathcal{G}_0^0(t) &= G_0^0(t) + \hat{G}_0^0(t) \\
\mathcal{G}_0^2(t) &= G_0^2(t) + \hat{G}_0^2(t) \\
\mathcal{G}_1^1(t) &= G_1^1(t) + \hat{G}_1^1(t) \\
\tilde{\mathcal{G}}_1^1(t) &= \tilde{G}_1^1(t) + \hat{\tilde{G}}_1^1(t) .
\end{aligned} \tag{3.9}$$

The “hat-functions” which appear in the expressions of the partial-waves are composed of a sum of angular integrals involving the one-variable functions, they are given in appendix C.1. The hat-functions carry the left-hand cuts of the partial-wave amplitudes. These cuts contain the negative real axis and have a complex component because of the unequal masses of the participating particles [41]. In addition, because $m_D > m_K + 2m_\pi$ the left-hand cuts have components on the positive real axis which overlap with the unitarity cut: in the region $(m_K + m_\pi)^2 \leq s \leq (m_D - m_\pi)^2$ for the s variable and $4m_\pi^2 \leq t \leq (m_D - m_K)^2$ for the t variable. The prescription for separating the unitarity cut from the left-hand cut in these regions is well known (e.g. [33] and references therein): one must add an infinitesimal imaginary part to the D mass, $m_D^2 \rightarrow m_D^2 + i\epsilon$, with $\epsilon > 0$, this is illustrated in fig. 3. The discontinuities of the one-variable functions across the unitarity cut are then simply equal to those of the partial-wave amplitudes given by unitarity. Keeping the elastic contribution to unitarity for the $\bar{K}\pi \rightarrow D\pi$ partial-wave amplitude one has

$$\text{disc}[F_j^K(s)] = \text{disc}[\mathcal{F}_j^K(s)] = \exp(-i\delta_j^K(s)) \sin(\delta_j^K(s)) \mathcal{F}_j^K(s) , \tag{3.10}$$

in which δ_j^K are the $\bar{K}\pi \rightarrow \bar{K}\pi$ scattering phase-shifts with isospin $K = 1/2, 3/2$. This relation gives the discontinuity across the unitarity cut, using analyticity, defining the discontinuity as

$$\text{disc}[\mathcal{F}_j^K(s)] \equiv \frac{\mathcal{F}_j^K(s+i\epsilon) - \mathcal{F}_j^K(s-i\epsilon)}{2i} . \quad (3.11)$$

The same unitarity relations hold for the amplitudes $\mathcal{H}_j^K(s)$. For the t -channel amplitudes $DK \rightarrow \pi\pi$, keeping the elastic contribution to unitarity one has

$$\text{disc}[G_j^I(t)] = \text{disc}[\mathcal{G}_j^I(t)] = \exp(-i\delta_j^I(t)) \sin(\delta_j^I(t)) \mathcal{G}_j^I(t) \quad (3.12)$$

which involves the $\pi\pi \rightarrow \pi\pi$ phase-shifts δ_j^I , with $I = 0, 1, 2$.

3.3 Khuri-Treiman equations for the D^+ and D^0 functions

The form of the discontinuities given in eqs. (3.10), (3.12) (which are based on elastic unitarity) allows one to express the one-variable functions with Muskhelishvili-Omnès (MO) dispersion relations [42, 43, 44] which exhibit the dependence on the scattering phase-shifts explicitly. A key ingredient is the Omnès function which is expressed as follows in terms of a given phase-shift ϕ ,

$$\Omega(w) = \exp\left(\frac{w}{\pi} \int_{w_{th}}^{\infty} dw' \frac{\phi(w')}{w'(w'-w)}\right) \quad (3.13)$$

where the threshold value w_{th} is $4m_\pi^2$ for $\pi\pi$ phases and $(m_K + m_\pi)^2$ for $K\pi$ and it has been assumed that the phase is bounded by a constant at infinity. We will further assume that this constant is a multiple of π . As is well known, the asymptotic behaviour of the Omnès function is related to that of the phase by,

$$\phi(w)|_{w \rightarrow \infty} = m\pi, \quad \Omega(w)|_{w \rightarrow \infty} \sim \frac{1}{w^m} . \quad (3.14)$$

Outside of the energy region where scattering is elastic the value of the phase to be used in the Omnès function is, in fact, arbitrary. We will assume the following asymptotic values, chosen to be a multiple of π close to the value of the phase-shift at the border of the inelasticity region⁴,

$$\begin{aligned} \delta_0^{1/2}(\infty) = \pi, \quad \delta_1^{1/2}(\infty) = \pi, \quad \delta_0^{3/2}(\infty) = 0, \quad \delta_1^{3/2}(\infty) = 0 \\ \delta_0^0(\infty) = \pi, \quad \delta_1^1(\infty) = \pi, \quad \delta_0^2(\infty) = 0 . \end{aligned} \quad (3.15)$$

Implementing the uniqueness conditions (3.5) as well as the assumed linear asymptotic behaviour, one can write the MO dispersive representations for the six D^+ functions as

⁴We differ here from ref. [21] who take $\delta_0^{1/2}(\infty) = 2\pi$.

follows

$$\begin{aligned}
F_0^{3/2}(w) &= \Omega_0^{3/2}(w) w^2 \widehat{I}_{0F}^{3/2}(2, w) \\
F_0^{1/2}(w) &= \Omega_0^{1/2}(w) \left[c_0 + c_1 w + c_2 w^2 + w^3 \widehat{I}_{0F}^{1/2}(3, w) \right] \\
F_1^{3/2}(w) &= \Omega_1^{3/2}(w) \widehat{I}_{1F}^{3/2}(0, w) \\
F_1^{1/2}(w) &= \Omega_1^{1/2}(w) \left[c_3 + w \widehat{I}_{1F}^{1/2}(1, w) \right] \\
G_0^2(t) &= \Omega_0^2(t) t^2 \widehat{I}_{0G}^2(2, t) \\
G_1^1(t) &= \Omega_1^1(t) \left[c_4 + c_5 t + t^2 \widehat{I}_{1G}^1(2, t) \right]
\end{aligned} \tag{3.16}$$

involving six polynomial parameters c_i . In these formulae the functions $\widehat{I}(n, z)$ are dispersive integrals with n subtractions involving the hat-functions (see eqs. (3.8), (3.9))

$$\begin{aligned}
\widehat{I}_{jF}^K(n, w) &= \frac{1}{\pi} \int_{(m_K+m_\pi)^2}^{\infty} \frac{\widehat{F}_j^K(w') \sin \delta_j^K(w')}{(w')^n (w' - w) |\Omega_j^K(w')|} dw' \\
\widehat{I}_{jG}^K(n, t) &= \frac{1}{\pi} \int_{4m_\pi^2}^{\infty} \frac{\widehat{G}_j^K(t') \sin \delta_j^K(t')}{(t')^n (t' - t) |\Omega_j^K(t')|} dt' .
\end{aligned} \tag{3.17}$$

such that eqs. (3.16) form a closed system of integral equations for the six F -functions. The \widehat{I} integrals contain final-state interaction effects which involve three particles induced by the two-body interactions described by the various phase-shifts. These integrals are complex functions, their imaginary parts being induced both by the $1/(w' - w)$ and $1/(t' - t)$ denominators when w, t approach the real axis from above and from the fact that the hat-functions are complex. The associated subtracted constants c_i must thus be complex as well and this generates deviations from Watson's theorem for the phases of the F -functions.

In the case of the D^0 amplitudes now, the six additional functions which are needed satisfy the following equations

$$\begin{aligned}
H_0^{3/2}(w) &= \Omega_0^{3/2}(w) w^2 \widehat{I}_{0H}^{3/2}(2, w) \\
H_0^{1/2}(w) &= \Omega_0^{1/2}(w) \left[d_0 + d_1 w + d_2 w^2 + w^3 \widehat{I}_{0H}^{1/2}(3, w) \right] \\
H_1^{3/2}(w) &= \Omega_1^{3/2}(w) \widehat{I}_{1H}^{3/2}(0, w) \\
H_1^{1/2}(w) &= \Omega_1^{1/2}(w) \left[d_3 + w \widehat{I}_{1H}^{1/2}(1, w) \right] \\
G_0^0(t) &= \Omega_0^0(t) \left[d_4 t^2 + t^3 \widehat{I}_{0G}^0(3, t) \right] \\
\widetilde{G}_1^1(t) &= \Omega_1^1(t) \left[d_5 + d_6 t + t^2 \widehat{I}_{1G}^1(2, t) \right] .
\end{aligned} \tag{3.18}$$

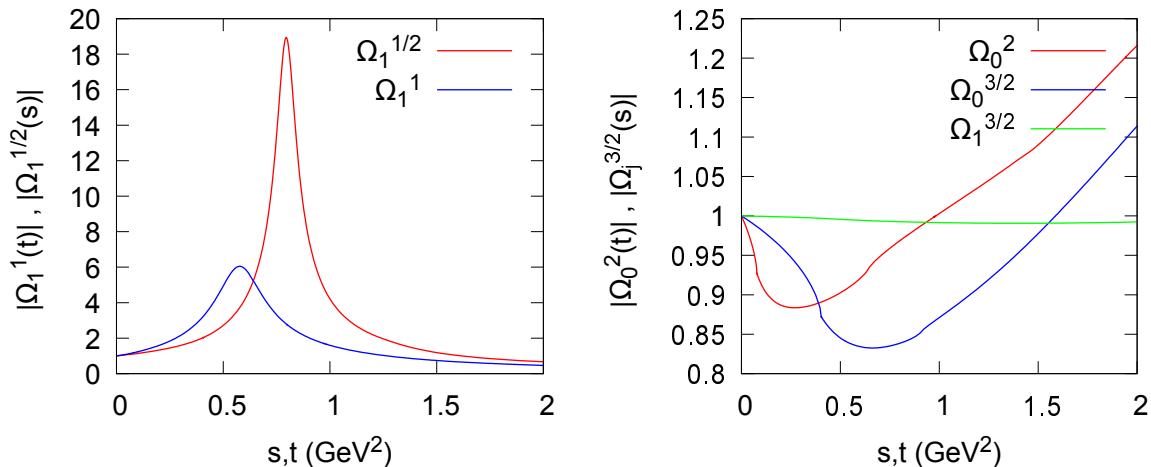


Figure 4: Left: Omnès functions (absolute values) for the $\pi\pi$ and πK P -waves. Right: Omnès functions with isospin $K = 3/2, I = 2$.

They involve 7 complex polynomial parameters d_i . The integrals \widehat{I}_{jH}^K have the same form as eqs. (3.17) replacing the \widehat{F}_j^K functions by \widehat{H}_j^K in the integrands. The expressions of the hat-functions $\widehat{H}_j^K, \widehat{G}_0^0, \widehat{G}_1^1$ in terms of angular integrals are given in eqs. (C.3), (C.7) in appendix C.1. They are linear combinations of the twelve one-variable functions.

The above equations have been derived starting from unitarity equations (3.10) (3.12) in which a single channel has been included (elastic approximation). Experimental studies of $\pi\pi$ and πK scattering suggest that this approximation should be valid in energy regions which include the prominent P -wave resonances $K^*(890)$ and $\rho(770)$ as well as the scalar resonance $K_0^*(1430)$ but not the $I = 0$ scalar $f_0(980)$. Obviously, as the energy increases, we expect that more channels should be taken into account. In cases where inelasticity sets in smoothly one can hope that their effects can be absorbed, to some extent, into the subtraction polynomials. This is not the case for the attractive S -waves in $\pi\pi$ or πK scattering for which inelastic scattering sets in sharply under the effect of the $f_0(980)$ and $K_0^*(1950)$ resonances respectively. We will describe below (sec. 4.2) an approximate procedure for taking this feature into account.

4 Solutions of the KT equations and fits to the data

4.1 πK and $\pi\pi$ phase-shifts and resonances

The $K^*(892)$ resonance plays a dominant role in all $D \rightarrow \bar{K}\pi\pi$ decays. Let us start by recalling some points concerning its properties. In the case of the $K^*(892)^0$ there is

good agreement between the values obtained from semi-leptonic D decays [45, 46, 47] (which are the cleanest channels, in principle) and those obtained from hadroproduction or other decays and the PDG [36] gives $M_{K^{*0}}, \Gamma_{K^{*0}} = (895.6 \pm 0.2, 47.3 \pm 0.5)$ MeV. For the $K^*(892)^+$ the most reliable determinations are from τ decays and the Belle collaboration [48] has obtained⁵ $M_{K^{*+}}, \Gamma_{K^{*+}} = (895.47 \pm 0.77, 46.2 \pm 1.34)$. One sees that isospin breaking effects are very small for the $K^*(892)$ which is a favourable point for our isospin symmetric approach. Determinations of πK scattering phase-shifts have been performed in a number of production experiments since the 70's (see e.g. [50] for a recent dispersive analysis and a list of references). A new set of measurements of this type using a K_L beam is planned at JLab [51]. We describe the $I = 1/2$ P -wave phase-shift based on a combined fit of the τ decay data of Belle [48] and the πK phase-shifts measurements of refs [52, 53] using a three-channel K -matrix from which the πK vector form-factor $f_+^{K\pi}$ as well as the phase-shifts can be computed [54].

Concerning the properties of the $\rho(770)$ resonance in the $\pi\pi$ P -wave, precise determinations have been derived from $e^+e^- \rightarrow \pi^+\pi^-$ and $\tau^- \rightarrow \pi^-\pi^0\nu_\tau$. Isospin breaking effects on the mass and the width again turn out to be smaller than 2 MeV. For the $\pi\pi$ P -wave phase-shift we use the Roy equations solutions provided in ref. [55] when $E \leq 0.8$ GeV, which are compatible with the e^+e^- and τ decay results. In the region $E > 0.8$ GeV we use simple fits to the phase-shift determination from ref. [56]. We compute the Omnès functions for both the $\pi\pi$ and πK elastic scattering phase-shifts. Fig. 4 (left) shows that they behave very similarly to Breit-Wigner functions. Scattering ceases to be purely elastic for energies above 1 GeV, approximately, for both $\pi\pi$ and πK in the P -wave. The inelastic effects set in smoothly and we assume that they can be partly absorbed into the polynomial parameters. Eventually, we will introduce a modification for πK by hand in the region of the $K^*(1680)$ resonance.

The channels with isospin $I = 3/2$ (for πK) and $I = 2$ (for $\pi\pi$) are repulsive. For the $I = 2$ S -wave phase-shift we use the Roy equations based parametrisation from ref. [55] below 0.8 GeV and a simple fit to the experimental data [57, 58] above, such that the phase shift goes to zero when $E \rightarrow \infty$. For the $I = 3/2$ S -wave a parametrisation with a simple rational function of the momentum as proposed in [59] provides a good fit to the experimental phase shift. Below 1 GeV we use a parametrisation constrained by the Roy-Steiner equations [60]. The $I = 3/2$ P -wave phase-shift is very small but it has been measured [52], we have used the parametrisation proposed in ref. [50]. The Omnès functions for these $I = 2$ and $I = 3/2$ channels are shown in fig. 4 (right).

⁵A compatible preliminary result was quoted by the Babar collaboration [49] $M_{K^{*+}}, \Gamma_{K^{*+}} = (894.57 \pm 0.27, 45.56 \pm 0.71)$ MeV.

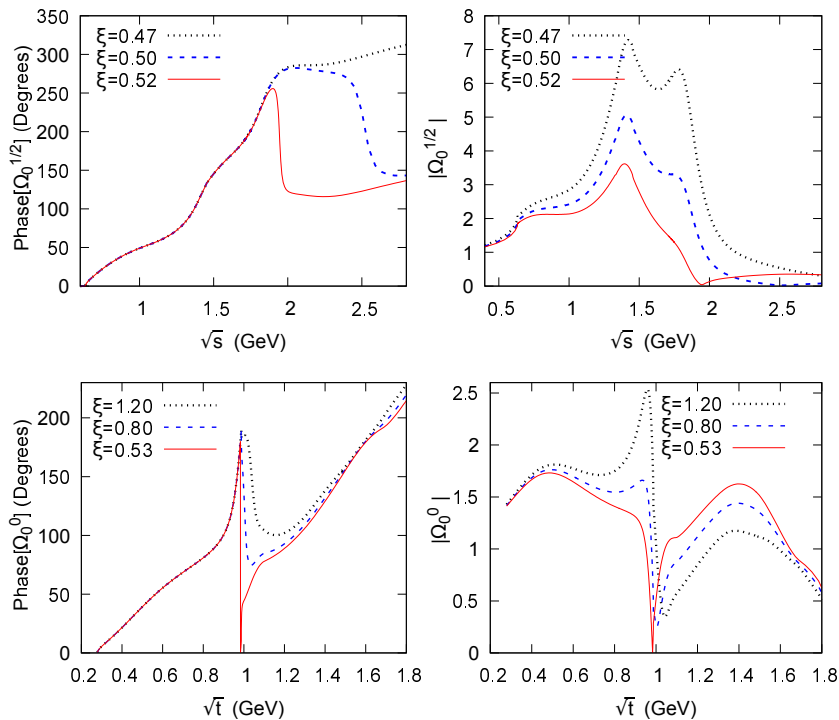


Figure 5: Omnès functions for the πK (upper plots) and $\pi\pi$ (lower plots) attractive S -waves generated from using two-channel MO matrices (see eq. (4.1)). The phases are displayed on the left plots and the absolute values on the right plots.

4.2 S -wave modelling in inelastic energy regions

Let us now turn to the S -waves with $I = 0$ and $I = 1/2$. For $\pi\pi$ scattering, a distinctive feature is that inelasticity remains negligibly small below 1 GeV and sets in sharply at the $K\bar{K}$ threshold, under the influence of the $f_0(980)$ resonance (e.g. [56]). A somewhat similar feature is seen in the πK experimental data [52, 53]. In that case, inelasticity remains very small below the $\eta'K$ threshold and then increases rapidly due to the $K_0^*(1950)$ resonance. Concerning the $D \rightarrow \bar{K}\pi\pi$ amplitudes, the physical effect of $\pi\pi \rightarrow K\bar{K}$ inelastic rescattering, for instance, is to introduce a coupling with the $D \rightarrow \bar{K}K\bar{K}$ amplitudes. A proper treatment is possible, in principle, in which the equation for the $I = 0$ function G_0^0 would be replaced by a system of two equations relating G_0^0 and the analogous function $G_{0,K\bar{K}}^0$ in the $D \rightarrow \bar{K}K\bar{K}$ amplitude. These equations would involve a 2×2 MO matrix instead of the one channel MO function. Here, we will use 2×2 MO matrices simply for generating a plausible phase to be used in a single channel function in the inelastic region.

We have determined two-channel T -matrices for both $\pi\pi$ and πK S -waves assuming the dominance of a single inelastic channel and using the experimental scattering

data up to 2 GeV. Taking appropriate asymptotic conditions, one can then compute corresponding two-channel MO matrices (see [61, 62] for early calculations of this type). Watson's theorem constrains the phases of the matrix elements of the first line, Ω_{1i} , to be equal to the elastic scattering phase in the elastic energy region. Forming linear combinations

$$\Omega_{eff}(z) = \Omega_{11}(z) + \xi\Omega_{12}(z) \quad (4.1)$$

(with ξ real) one obtains a family of one-channel Omnès functions which differ in the behaviour of the phase in the inelastic region. We have considered values of ξ such that the asymptotic value of the phase is equal to π for both $\pi\pi$ and πK , as assumed in eqs. (3.15). The phase of Ω_{eff} is illustrated in fig. 5 for $\pi\pi$ and πK scattering. This procedure eventually generates a sharp drop of the phase above the inelastic threshold. For πK , a similar drop was experimentally observed in the phase of the πK scalar component of the $D^+ \rightarrow K^-\pi^+\pi^+$ amplitude [63, 13, 64]. Correspondingly, the peak of the $K^*(1950)$ resonance can be strongly reduced (see fig. 5). We will argue in appendix A that the soft pion theorems for the $D \rightarrow \bar{K}\pi\pi$ amplitudes support such a reduction.

4.3 Matrix approximations to the KT equations

We will formulate the KT equations such as to determine the one-variable functions on a discrete set of points,

$$(m_K + m_\pi)^2 \leq s_1 < s_2 < \dots < s_N \quad (4.2)$$

for the variables s, u , where s_N is a sufficiently large value, and

$$4m_\pi^2 \leq t_1 < t_2 < \dots < t_M \quad (4.3)$$

for the t variable. We consider first the F -functions and introduce two vectors of size $4N + 2M$ containing the values of the one-variable functions at the points s_i, t_i and the values of the corresponding hat-functions,

$$\mathbb{F} \equiv \begin{pmatrix} F_0^{3/2}(s_i) \\ F_0^{1/2}(s_i) \\ F_1^{3/2}(s_i) \\ F_1^{1/2}(s_i) \\ G_0^2(t_i) \\ G_1^1(t_i) \end{pmatrix}, \quad \widehat{\mathbb{F}} \equiv \begin{pmatrix} \widehat{F}_0^{3/2}(s_i) \\ \widehat{F}_0^{1/2}(s_i) \\ \widehat{F}_1^{3/2}(s_i) \\ \widehat{F}_1^{1/2}(s_i) \\ \widehat{G}_0^2(t_i) \\ \widehat{G}_1^1(t_i) \end{pmatrix}. \quad (4.4)$$

We now write the KT integral equations (3.16) (3.18) using an approximate evaluation of the \widehat{I} integrals. The integrands have singularities but it can be shown that the integrals are well defined and finite by deforming the integration contour in the complex

plane [33, 65]. Our method uses real axis integration, which is fast and convenient, and we have checked that it correctly reproduces the high-accuracy results derived for $\eta \rightarrow 3\pi$ in ref. [65]. Let us illustrate our procedure in the case of the integral $\widehat{I}_{0F}^{3/2}$. We wish to approximate this integral by a discrete sum as a function of $\widehat{F}_0^{3/2}(s_{n'})$. The integrand has a Cauchy singularity $1/(s' - s)$ and, in addition, the function $\widehat{F}_0^{3/2}(s')$ has a square-root singularity when $s' \rightarrow s_D^- = (m_D - m_\pi)^2$ (see [33] and appendix C.2). We multiply and divide the integrand by $\sqrt{s_D^- - s'}$ and define

$$\psi_0^{3/2}(s') \equiv \frac{\sin \delta_0^{3/2}(s')}{(s')^2 |\Omega_0^{3/2}(s')|} \sqrt{s_D^- - s'} \widehat{F}_0^{3/2}(s') \quad (4.5)$$

which is a finite and continuous function of s' in the whole integration range. Therefore it can be accurately approximated by a linear function in the small range $[s_{n'}, s_{n'+1}]$. The integration in this range can be performed using the analytical evaluation of the singular integrals

$$\int_{s_a}^{s_b} \frac{ds'}{\sqrt{s_D^- - s'}(s' - z)} = I_0(s_b, z) - I_0(s_a, z) \quad (4.6)$$

with

$$I_0(s', z) = \frac{1}{\sqrt{s_D^- - z}} \left[\log(z - s') - \log \left(\sqrt{s_D^- - s'} + \sqrt{s_D^- - z} \right)^2 \right]. \quad (4.7)$$

Summing the integrals over the ranges $[s_{n'}, s_{n'+1}]$ we obtain an approximation of $\widehat{I}_{0F}^{3/2}(2, s)$ as a discrete sum

$$\widehat{I}_{0F}^{3/2}(2, s) \simeq \frac{1}{\pi} \sum_{n'=1}^{N_s} \widehat{W}_0^{(n')}(s) \psi_0^{3/2}(s_{n'}) \widehat{F}_0^{3/2}(s_{n'}) \quad (4.8)$$

in which the integration weights have the following expression⁶

$$\begin{aligned} \widehat{W}_0^{(n')}(s) &= \frac{s_{n'+1} - s}{s_{n'+1} - s_{n'}} I_0(s_{n'+1}, s) + \frac{s_{n'-1} - s}{s_{n'} - s_{n'-1}} I_0(s_{n'-1}, s) \\ &+ \frac{(s_{n'+1} - s_{n'-1})(s - s_{n'})}{(s_{n'} - s_{n'-1})(s_{n'+1} - s_{n'})} I_0(s_{n'}, s) \\ &+ 2 \left(\frac{1}{\sqrt{s_D^- - s_{n'}} + \sqrt{s_D^- - s_{n'-1}}} - \frac{1}{\sqrt{s_D^- - s_{n'}} + \sqrt{s_D^- - s_{n'+1}}} \right). \end{aligned} \quad (4.9)$$

Replacing all the \widehat{I} integrals in the set of integral equations (3.16) by their analogous discretised approximations one obtains a matrix approximation to these equations

$$\mathbb{F} = \mathbb{F}_{(0)} + \mathcal{W}_I^F \times \widehat{\mathbb{F}} \quad (4.10)$$

⁶This formula is for generic values of n' . For $n' = 1$ or $n' = N_s$ it has to be modified.

where $\mathbb{F}_{(0)}$ contains the dependence on the c_i parameters

$$\mathbb{F}_{(0)} = \begin{pmatrix} 0 \\ \Omega_0^{1/2}(s_i)(c_0 + c_1 s_i + c_2 s_i^2) \\ 0 \\ \Omega_1^{1/2}(s_i)c_3 \\ 0 \\ \Omega_1^1(t_i)(c_4 + c_5 t_i) \end{pmatrix}. \quad (4.11)$$

A similar procedure can be used in order to generate discretised approximations to the angular integrals. Consider, for example, $\langle F_0^{3/2}(u) \rangle_s$. At first, we express the angular integral as an integral over the right-hand cut (using the ordinary dispersive representations, see appendix C.2)

$$\langle F_0^{3/2}(u) \rangle_s = -\frac{1}{\pi} \int_{(m_K+m_\pi)^2}^{\infty} K_u^0(s, u') \text{disc}[F_0^{3/2}(u')] du' \quad (4.12)$$

this will allow us to use the same grid points s_i and t_i as above. The integrand in eq. (4.12) has logarithmic singularities coming from kernel $K_u^0(s, u')$ at $u' = u^\pm(s)$ (see (C.20)) and a square-root singularity from $\text{disc}[F_0^{3/2}(u')]$ at $u' = s_D^-$. As before, we multiply and divide by $\sqrt{s_D^- - u'}$ and, using the unitarity relation to express the discontinuity, we get

$$\langle F_0^{3/2}(u) \rangle_s = -\frac{1}{\pi} \int_{(m_K+m_\pi)^2}^{\infty} \frac{K_u^0(s, u')}{\sqrt{s_D^- - u'}} \left[\phi_0^{3/2}(u') \left(F_0^{3/2}(u') + \widehat{F}_0^{3/2}(u') \right) \right] \quad (4.13)$$

with

$$\phi_0^{3/2}(u') = \exp(-i\delta_0^{3/2}(u')) \sin(\delta_0^{3/2}(u')) \sqrt{s_D^- - u'}. \quad (4.14)$$

The quantity inside the square brackets in the integrand of eq. (4.13) is finite and continuous and one can use linear approximations in the small ranges $[s_{n'}, s_{n'+1}]$. The singular integration part which involves logarithms can be written using the same function I_0 which appeared above (4.7)

$$\int_{s_a}^{s_b} \frac{\log(u' - u_\pm(s))}{\sqrt{s_D^- - u'}} du' = -2\sqrt{s_D^- - u'} \log(u' - u_\pm(s)) + 2(s_D^- - u') I_0(u', u_\pm(s)) \Big|_{s_s}^{s_b}. \quad (4.15)$$

It is then not difficult to generate a set of weights which enable one to express the angular average $\langle F_0^{3/2}(u) \rangle_s$ in terms of $F_0^{3/2}(s_{n'}) + \widehat{F}_0^{3/2}(s_{n'})$. Repeating this procedure for the other angular averages and then forming the linear combinations which give the hat-functions we obtain a second set of linear equations which have the following form

$$\widehat{\mathbb{F}} = \widehat{\mathbb{F}}_{(0)} + \mathcal{W}_K^F \times (\mathbb{F} + \widehat{\mathbb{F}}) \quad (4.16)$$

where the first term on the right-hand side is generated from the subtraction constants in the ordinary dispersive representations

$$\widehat{\mathbb{F}}_{(0)} = \begin{pmatrix} \frac{1}{3}(c_0 - c_4 s_i) + \frac{1}{6}(c'_1 + c_4)(\Sigma - s_i + \frac{\Delta}{s_i}) \\ \frac{1}{3}(2c_0 + c_4 s_i) + \frac{1}{6}(2c'_1 - c_4)(\Sigma - s_i + \frac{\Delta}{s_i}) \\ -\frac{1}{6s_i}(c'_1 + c_4) \\ -\frac{1}{6s_i}(2c'_1 - c_4) \\ -\sqrt{2}(2c_0 + c'_1(\Sigma - t_i)) \\ \frac{1}{2}c'_1 \end{pmatrix} \quad (4.17)$$

and contains the dependence on the parameters c_i . Those appear only in the terms $\mathbb{F}_{(0)}$ and $\widehat{\mathbb{F}}_{(0)}$, it is then obvious that the solutions of the system of equations (4.10), (4.16) are linear functions of c_i . A set of six independent solutions can be determined setting one of the c_i parameters equal to 1 and the others equal to 0.

Let us now consider the H -functions and introduce the corresponding vectors

$$\mathbb{H} \equiv \begin{pmatrix} H_0^{3/2}(s_i) \\ H_0^{1/2}(s_i) \\ H_1^{3/2}(s_i) \\ H_1^{1/2}(s_i) \\ G_0^0(t_i) \\ \widetilde{G}_1^1(t_i) \end{pmatrix}, \quad \widehat{\mathbb{H}} \equiv \begin{pmatrix} \widehat{H}_0^{3/2}(s_i) \\ \widehat{H}_0^{1/2}(s_i) \\ \widehat{H}_1^{3/2}(s_i) \\ \widehat{H}_1^{1/2}(s_i) \\ \widehat{G}_0^0(t_i) \\ \widehat{\widetilde{G}}_1^1(t_i) \end{pmatrix}. \quad (4.18)$$

The first matrix equation is analogous to (4.10)

$$\mathbb{H} = \mathbb{H}_{(0)} + \mathcal{W}_F^H \times \widehat{\mathbb{H}} \quad (4.19)$$

where $\mathbb{H}_{(0)}$ contains the parameters d_i

$$\mathbb{H}_{(0)} = \begin{pmatrix} 0 \\ \Omega_0^{1/2}(s_i)(d_0 + d_1 s_i + d_2 s_i^2) \\ 0 \\ \Omega_1^{1/2}(s_i) d_3 \\ \Omega_0^0(t_i)(d_4 t_i^2) \\ \Omega_1^1(t_i)(d_5 + d_6 t_i) \end{pmatrix}. \quad (4.20)$$

The extra set of equations generated from the expressions of the \widehat{H} function are similar to eqs. (4.16)

$$\widehat{\mathbb{H}} = \widehat{\mathbb{H}}_{(0)} + \mathcal{W}_K^{HF} \times (\mathbb{F} + \widehat{\mathbb{F}}) + \mathcal{W}_K^{HH} \times (\mathbb{H} + \widehat{\mathbb{H}}). \quad (4.21)$$

albeit slightly more complicated due to the contributions from both the F and the H functions (see eqs. (C.3) (C.7)). The vector $\widehat{\mathbb{H}}_{(0)}$ depends on both the c_i and the d_i parameters.

$$\widehat{\mathbb{H}}_{(0)} = \begin{pmatrix} \frac{1}{3}(d_0 - \sqrt{2}d_5 s_i) + \frac{1}{6}(d'_1 + \sqrt{2}d_5)(\Sigma - s_i + \frac{\Delta}{s_i}) \\ \frac{1}{3}(-d_0 + \sqrt{2}(c_0 - (c_4 - 4d_5)s_i) + \frac{1}{6}(-d'_1 + \sqrt{2}(c'_1 + c_4 - 4d_5))(\Sigma - s_i + \frac{\Delta}{s_i}) \\ -\frac{1}{6s_i}(d'_1 + \sqrt{2}d_5) \\ -\frac{1}{6s_i}(-d'_1 + \sqrt{2}(c'_1 + c_4 - 4d_5)) \\ \frac{1}{3}(-\sqrt{2}c_0 + 3d_0) + \frac{1}{6}(-\sqrt{2}c'_1 + 3d'_1)(\Sigma - t_i) \\ \frac{\sqrt{2}}{4}d'_1 \end{pmatrix}. \quad (4.22)$$

The H -functions are linear in the c_i and d_i parameters, a set of 6+7 independent solutions is generated by setting one of these parameters equal to 1 and the others to 0 in the RS equations.

The numerical results presented below use values for the number of points $N \sim M \sim 700 - 800$ and, for the upper integration ranges, $s_N \sim t_M = 10^3 \text{ GeV}^2$. The matrices which appear in the discretised form of the RS equations (4.10) (4.19) are then rather large but they turn out to be well conditioned and solving the linear equations does not cause any problem. As a check, we have verified that we could reproduce the results of ref. [21] on the independent solutions when using the same input phase-shifts. We have also verified that the solutions obey ordinary dispersion relations. Once one has determined the set of independent solutions, using them to perform fits is just as easy as with a simple isobar model because of the linearity in the parameters c_i, d_i . Such fits will be discussed below.

4.4 D^+ fits

We will first test our model against the measurements performed by the BESIII collaboration [28] on the $D^+ \rightarrow K_S \pi^0 \pi^+$ mode. The Dalitz plot is divided into 1342 equal-size bins and the data consist of a set of values for the number of events in each bin: $N_i, \Delta N_i$. These numbers are corrected for the background, detector acceptance and energy resolution effects, such that they can be compared directly to a given theoretical model.

We will perform fits over the complete Dalitz plot, i.e. going beyond the region in which $2 \rightarrow 2$ rescattering can be considered as elastic. This will be necessary later on for addressing the available D^0 data, because the sizes and shapes of the bins, in that case, do not allow to separate the elastic from the inelastic regions. A further advantage is that this makes it possible to compute decay widths. As already mentioned the important vector and scalar resonances, with the exception of the $f_0(980)$, fall within

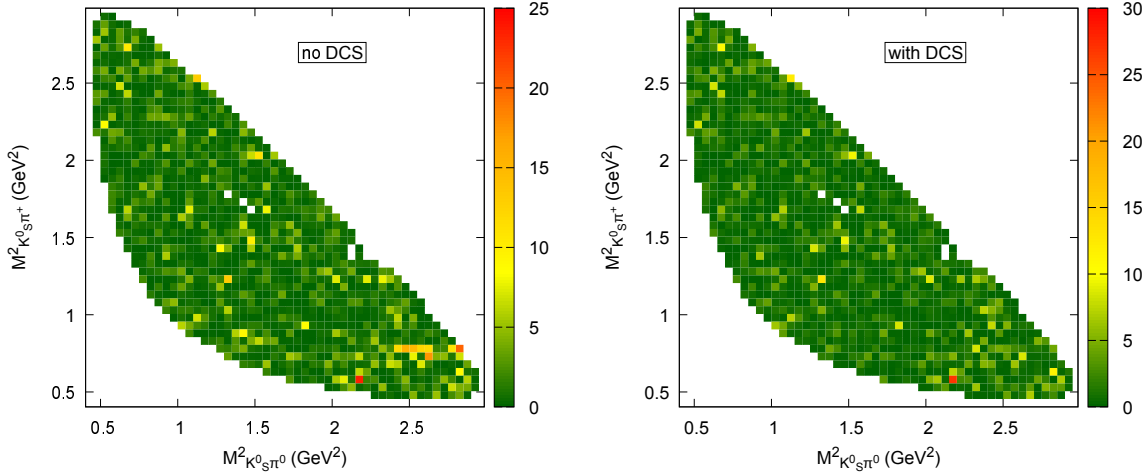


Figure 6: Distributions of the χ^2 values in the $D^+ \rightarrow K_S \pi^0 \pi^+$ fits. Left plot: no DCS contribution, right-plot: the DCS contribution is included in the fit.

the region of validity of elastic rescattering. The few smaller contributions which we add are described with a simple isobar model approach. At first, since a K_S is detected, a DCS amplitude must be considered which we assume to be dominated by the $K^*(892)^+$ resonance contribution. We also include the effect of the D -wave resonance $K_2^*(1430)$ and that of the P -wave resonance $K^*(1680)$. Our model for the $D^+ \rightarrow K_S \pi^0 \pi^+$ amplitude, finally, is as follows⁷

$$\begin{aligned}
\mathcal{A}_{D^+ \rightarrow K_S \pi^0 \pi^+} = & \frac{F_{norm}}{\sqrt{2}} \left\{ -2[F_0^{3/2}(s) + Z_s F_1^{3/2}(s)] + F_0^{1/2}(s) \right. \\
& + Z_s [F_1^{1/2}(s) + C_{K^*(1680)} BW_{K^*(1680)}(s)] + Z_{2s} C_{K_2^*(1430)} BW_{K_2^*(1430)}(s) \\
& \left. + 3[F_0^{3/2}(u) + Z_u F_1^{3/2}(u)] - \frac{\sqrt{2}}{4} G_0^2(t) + (s-u) G_1^1(t) + Z_u C_{DCS} BW_{K^*(892)}(u) \right\}
\end{aligned} \tag{4.23}$$

where the Breit-Wigner functions, called BW , are described in appendix C.3. In addition to the polynomial parameters c_i which drive the KT amplitudes, it involves the three complex resonance couplings $C_{K^*(1680)}$, $C_{K_2^*(1430)}$ and C_{DCS} also to be determined from the fit. The angular function Z_{2s} associated with the spin 2 resonance $K_2^*(1430)$, proportional to the Legendre polynomial $P_2(z_s)$, is given in eq. (2.39).

When performing the fit, it is convenient to fix one of the polynomial parameters c_i (we will set $c_3 = -1$) and introduce instead an overall normalisation factor F_{norm} . In

⁷We take $|K_{S,L}\rangle = (|K^0\rangle \pm |\bar{K}^0\rangle)/\sqrt{2}$, ignoring CP violation.

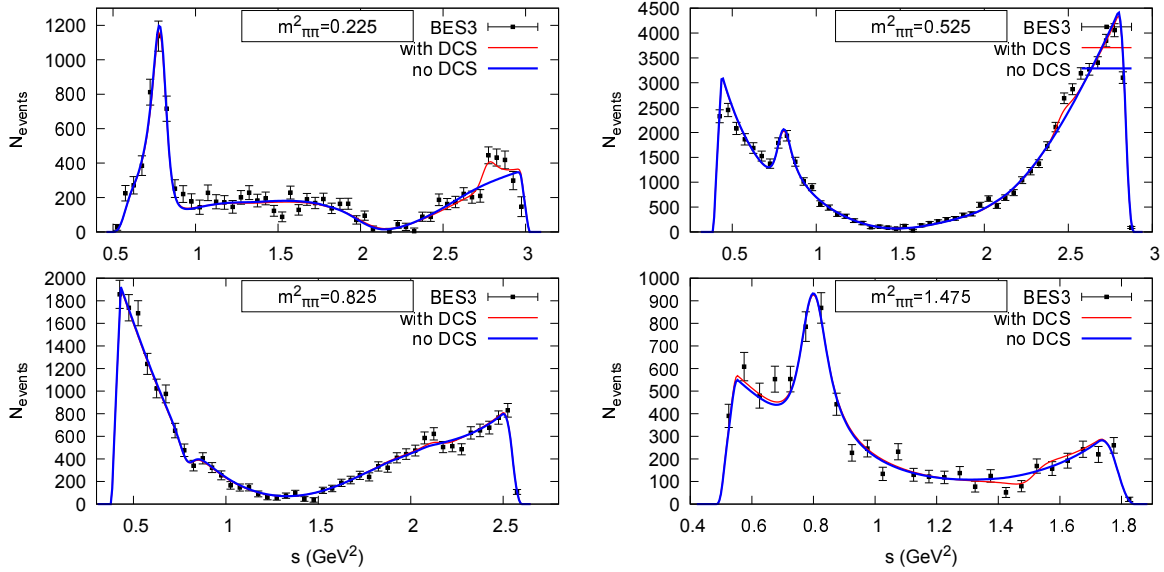


Figure 7: Comparison of the fitted amplitude with the experimental data along slices of Dalitz plot with fixed values of $t = m_{\pi\pi}^2$.

the fitting process F_{norm} is adjusted to the total number of experimental events while the physical value of F_{norm} can be determined from the experimental value of the width $\Gamma_{D^+ \rightarrow K_S \pi^0 \pi^+}$ (see below). In the calculation of the χ^2 we integrate the absolute value of the amplitude squared over each bin, dropping the bins which overlap with the boundary of the Dalitz plot, which leaves $N_{bins} = 1182$. At first, we ignore the DCS amplitude i.e. we set $C_{DCS} = 0$. We then have $N_{par} = 15$ parameters to fit. An additional parameter is ξ which, via eq. (4.1), controls the behaviour of the πK S -wave phase in the inelastic region. It is not included in the fit but its value is tuned to optimise the result, which gives $\xi \simeq 0.515$. Minimising the χ^2 we obtain

$$\chi^2 = 1576, \quad \chi^2/N_{dof} = 1.35 \quad (4.24)$$

which is comparable to the result of the fit reported in ref. [28] ($\chi^2/N_{dof} = 1.41$ with model A) using a substantially larger number of parameters $N_{par} = 25$. Fig. 6 (left) shows the distribution of the χ^2 values across the Dalitz plot. One can clearly see that there is a cluster of high χ^2 values corresponding to the mass of the $K^*(892)^+$. Including now the DCS contribution, the fit gives a significantly lower χ^2

$$\chi^2 = 1422, \quad \chi^2/N_{dof} = 1.22 \quad (4.25)$$

and fig. 6 (right) shows that, now, the high χ^2 values are isolated and randomly distributed across the Dalitz plot. There are obviously other DCS contributions which must be present: for instance $D^+ \rightarrow K^*(892)^0 \pi^+$ or $D^+ \rightarrow K^0 \rho^+$ but they cannot

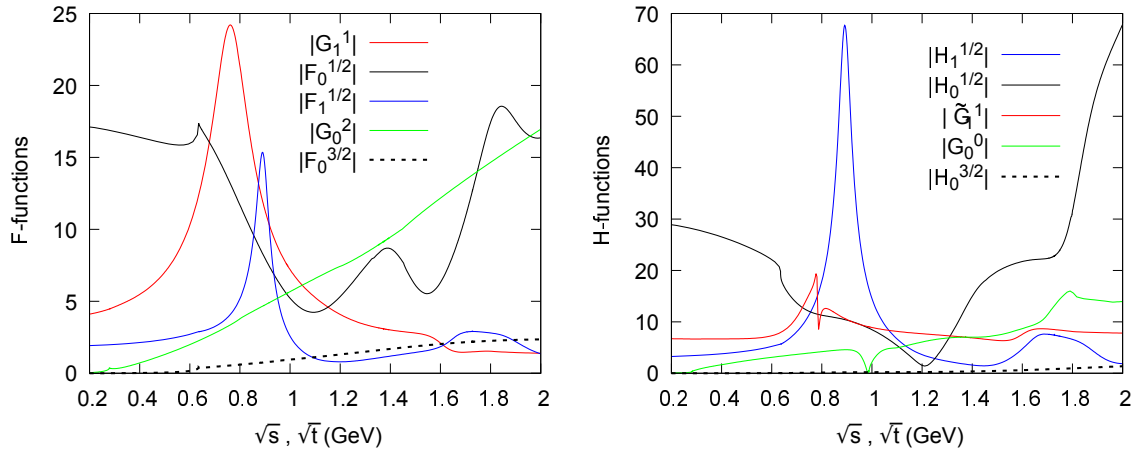


Figure 8: Left plot: absolute values of the F -functions resulting from the fit (central values). Right plot: the corresponding results for the H -functions. The small amplitudes $|F_1^{3/2}| \lesssim 0.04$, $|H_1^{3/2}| \lesssim 0.008$ are not shown.

be isolated using only data on the $D^+ \rightarrow K_S \pi^0 \pi^+$ mode. In principle, they could be determined thanks to the isospin symmetry, using an additional set of experimental data on the mode $D^+ \rightarrow K^- \pi^+ \pi^+$ (which has no DCS contributions) or using data on $D^+ \rightarrow K_L \pi^0 \pi^+$ decay. Further resonances like $K_3^*(1780)$ or $\rho(1450)$ have been considered in ref. [28], but we seem to find no need for them. One can also see from fig. 6 that the quality of the fit is similar in the regions where rescattering is elastic and in the regions where it is not. The quality of the fit and the role of the DCS amplitudes are illustrated on fig. 7 which shows slices of the Dalitz plot with fixed values of the $\pi\pi$ invariant mass. The values of the 17 parameters which result from our fit are collected in table 1. We note that the Cabibbo suppressed parameter $|C_{DCS}/c_3| \simeq 0.13$ is consistent in size with the value of the ratio of CKM parameters, $|V_{cd}V_{us}/V_{cs}V_{ud}| = 0.052 \pm 0.001$.

Fig. 8 (left) illustrates the magnitudes of the F -functions corresponding to the central values of the fitted parameters. The definitions of these functions, we recall, assume the fixing conditions (3.5). One notices the rather large size of the $I = 2$ amplitude G_0^2 . These results are similar to those obtained in ref. [24]. In particular, the function $F_0^{1/2}$ displays a large cusp at the πK threshold and has a first minimum close to 1 GeV followed by a maximum around 1.4 GeV. Using the parameters from table 1 one can evaluate the integral

$$I_{A2} = \frac{1}{256\pi^3 m_D^3} \int ds dt |\mathcal{A}_{D^+ \rightarrow K_S \pi^0 \pi^+}(s, t, u)|^2 = (9.583 \pm 0.029) \cdot 10^{-3} \text{ GeV} \quad (4.26)$$

from which the physical value of the normalisation factor F_{norm} can be determined

Parameter	Modulus		Phase(radians)
F_{norm}	8365.8 ± 91.3		-
c_0	17.15 ± 0.78		-2.63 ± 0.04
c_1	21.95 ± 1.12	GeV^{-2}	0.29 ± 0.05
c_2	4.69 ± 0.27	GeV^{-4}	-2.80 ± 0.06
c_3	1	GeV^{-4}	π
c_4	3.64 ± 0.27	GeV^{-2}	-2.06 ± 0.07
c_5	1.90 ± 0.45	GeV^{-4}	-0.72 ± 0.27
$C_{K_2^*(1430)}$	0.031 ± 0.003	GeV^{-6}	0.13 ± 0.15
$C_{K^*(1680)}$	1.91 ± 0.09	GeV^{-2}	2.52 ± 0.03
C_{DCS}	0.13 ± 0.01	GeV^{-2}	1.24 ± 0.09

Table 1: Values of the parameters entering the $D^+ \rightarrow \bar{K}\pi\pi$ amplitudes resulting from the fit to the data from ref. [28].

using [36]

$$|F_{norm}|^2 I_{A2} = \Gamma_{D^+ \rightarrow K_S \pi^0 \pi^+}^{exp} = (4.69 \pm 0.14) \cdot 10^{-14} \text{ GeV} , \quad (4.27)$$

which gives

$$F_{norm}(phys.) = (2.212 \pm 0.031) \cdot 10^{-6} . \quad (4.28)$$

This determination of $F_{norm}(phys.)$ is useful for discussing the soft pion limits relations (see appendix A). A prediction can be made for the decay width of the mode $D^+ \rightarrow K^- \pi^+ \pi^+$. Introducing the ratio of the widths

$$\mathcal{R} \equiv \frac{\Gamma(D^+ \rightarrow K^- \pi^+ \pi^+)}{\Gamma(D^+ \rightarrow K_S \pi^0 \pi^+)} \quad (4.29)$$

the model predicts

$$\mathcal{R}^{model} = 1.235 \pm 0.013 \quad (4.30)$$

which is compatible with the experimental value [36]

$$\mathcal{R}^{exp} = 1.274 \pm 0.042 . \quad (4.31)$$

4.5 D^0 fits

From the D^+ fits discussed above, we have determined the parameters of the F -functions, we now want to determine the analogous parameters of the H -functions using D^0 decay inputs. Of the three possible decay modes, the mode $D^0 \rightarrow K_S \pi^- \pi^+$ has attracted much interest because of its connection to the BPGGSZ [7] approach for measuring the angle γ/ϕ_3 . Dalitz plot data for $D^0 \rightarrow K_S \pi^- \pi^+$ on three different binnings have been published [29, 30], which we can use for our purposes. The first binning is called ‘‘Equal

$\Delta\delta_D$ ”, it is defined such that for s, u in bin i the phase difference $\Delta\delta_D(s, u)$ (defined in eq. (1.1)) lies between the two values

$$\frac{2\pi}{8}(i - \frac{3}{2}) \leq \Delta\delta_D(s, u) < \frac{2\pi}{8}(i - \frac{1}{2}), \quad (4.32)$$

with $i = 1, \dots, 8$. Fig. 9 shows the shapes of the bins computed using the Babar amplitude model [66]. The other two binnings are called “Optimal” and “Modified Optimal” they have been generated in ref. [67] from variations of the “Equal $\Delta\delta$ ”, binning such as to further optimise the determination of γ/ϕ_3 in the BPGGSZ method.⁸ The “Modified Optimal” binning is also shown in fig. 9.

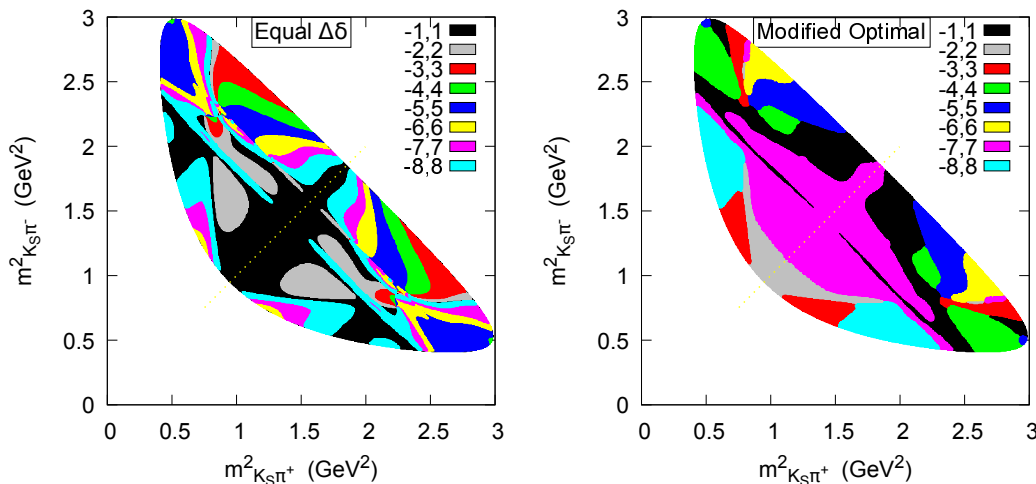


Figure 9: Illustration of two of the binnings used in the measurements of refs. [29, 30].

Refs. [29, 30] provide measures of three different observables, F_i , \bar{c}_i , \bar{s}_i , in each bin. F_i , at first, is the normalised number of events in bin i ,

$$F_i = \frac{N_i}{\sum_{-8}^8 N_i}, \quad N_i = \int_{bin_i} dsdu |\mathcal{A}_D(s, t, u)|^2 \quad (4.33)$$

One notes that the sums

$$S_- \equiv \sum_{i<0} F_i \simeq 0.25, \quad S_+ \equiv \sum_{i>0} F_i \simeq 0.75 \quad (4.34)$$

refer to halves of the Dalitz plot and are thus the same for the three binnings. The numerical values in eq. (4.34), taken from [30], indicate that the $K^*(892)^-$ resonance is

⁸The description of these binnings is provided in the form of “lookup tables” containing 53842 equally-spaced points in which each point is attributed an index label.

located in the region where the bins have a positive index $i > 0$, which must therefore satisfy $m_{K_S\pi^-}^2 < m_{K_S\pi^+}^2$, i.e. $s < u$ (contrary to what is stated in [30]). The quantities \bar{c}_i, \bar{s}_i are averages involving the cosine and the sine of the phase difference $\Delta\delta_D$,

$$\begin{aligned}\bar{c}_i &= \frac{\int_{bin_i} dsdu |\mathcal{A}_D(s, t, u)\mathcal{A}_D(u, t, s)| \cos \Delta\delta_D(s, u)}{\sqrt{N_i N_{-i}}} \\ \bar{s}_i &= \frac{\int_{bin_i} dsdu |\mathcal{A}_D(s, t, u)\mathcal{A}_D(u, t, s)| \sin \Delta\delta_D(s, u)}{\sqrt{N_i N_{-i}}}.\end{aligned}\tag{4.35}$$

Using the Schwartz inequality

$$\begin{aligned}\left(\int_{bin_i} dsdu |\mathcal{A}_D(s, t, u)\mathcal{A}_D(u, t, s)| \cos \Delta\delta_D(s, u)\right)^2 \leq \\ \int_{bin_i} dsdu |\mathcal{A}_D(s, t, u)|^2 \int_{bin_i} dsdu |\mathcal{A}_D(u, t, s)|^2 \cos^2 \Delta\delta_D(s, u),\end{aligned}\tag{4.36}$$

one easily deduces that \bar{c}_i and \bar{s}_i must lie inside a circle [68]

$$\bar{c}_i^2 + \bar{s}_i^2 \leq 1.\tag{4.37}$$

As one can see from fig 9, each bin has an intricate structure, extending over several regions of the Dalitz plot. In order to address the experimental results it is necessary for the model to be applicable in the whole Dalitz plot. As we did above, inelasticity effects are simulated in the πK and $\pi\pi$ attractive S -waves by generating a phase in the inelastic region using a two-channel Omnès matrix (see eq. (4.1)). We also add a few resonance contributions to the KT amplitudes. In addition to the $K^*(1680)$ and $K_2^*(1430)$ which were considered above, we now also include the $f_2(1270)$ which couples to $(\pi\pi)_{I=0}$. One also has to account for the isospin violating contribution from the $\omega(782)$ coupling to $\pi^+\pi^-$. We finally describe the DCS amplitude as before via a $K^*(892)^+$ Breit-Wigner function. There are clear indications that further contributions are required in this amplitude (see below) but it is necessary to keep the number of parameters to be as small as possible, due to the limited number of bins. Not including them obviously introduces some bias in the determination of the parameters of the CA amplitude. The $D^0 \rightarrow K_S\pi^-\pi^+$ amplitude, finally, is described as follows,

$$\begin{aligned}\mathcal{A}_{D^0 \rightarrow K_S\pi^-\pi^+}(s, t, u) &= \frac{F_{norm}}{\sqrt{2}} \left\{ \sqrt{2}(F_0^{3/2}(s) + Z_s F_1^{3/2}(s)) \right. \\ &\quad - (H_0^{3/2}(s) + Z_s H_1^{3/2}(s)) - 3(H_0^{3/2}(u) + Z_u H_1^{3/2}(u)) \\ &\quad - [H_0^{1/2}(s) + Z_s(H_1^{1/2}(s) + D_{K^*(1680)} BW_{K^*(1680)}(s)) \\ &\quad + Z_{2s} D_{K_2^*(1430)} BW_{K_2^*(1430)}(s)] + \frac{1}{6} G_0^2(t) - G_0^0(t) - Z_{2t} D_{f_2(1270)} BW_{f_2(1270)}(t) \\ &\quad \left. - (s - u) [\sqrt{2} \tilde{G}_1^1(t) + D_{\omega(892)} BW_{\omega(892)}(t)] + D_{DCS} Z_u BW_{K^*(892)}(u) \right\}\end{aligned}\tag{4.38}$$

where the angular function Z_{2t} is given in eq. (2.39). The physical value of F_{norm} has been determined from D^+ decays and is given in eq. (4.28). One observes that the F -functions play a relatively minor role in this amplitude since only $F_0^{3/2}$, $F_1^{3/2}$ and G_0^2 appear, which do not involve resonances. For this reason, it is interesting to also consider other D^0 amplitudes which probe different interferences between the F and the H -functions. We will use below the experimental decay widths for the three modes $K_S\pi^-\pi^+$, $K^-\pi^0\pi^+$ and $K_S\pi^0\pi^0$.

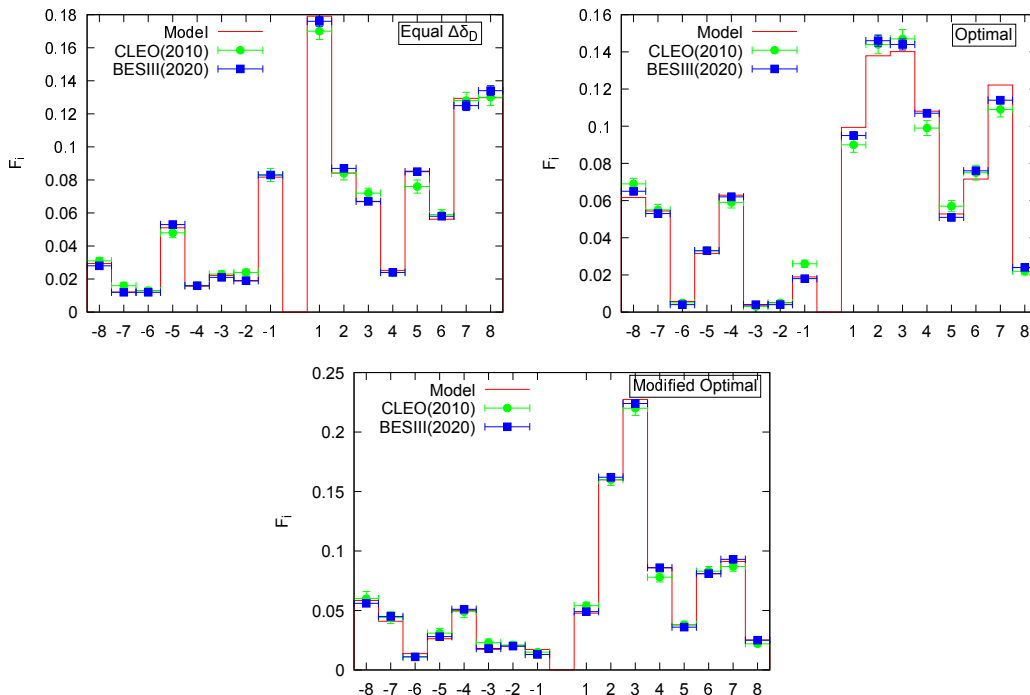


Figure 10: Normalised number of events F_i in each bin of three binnings. The experimental results are from ref. [30] (blue squares) and ref. [29] (green circles). The horizontal error bars are only to show the extent of a bin. The results from our amplitude after fitting the 24 parameters is represented by the red curve.

The free parameters in the D^0 amplitudes are: the polynomial coefficients d_0, \dots, d_6 , the coefficients of the Breit-Wigner functions $D_{K_2^*(1430)}$, $D_{K^*(1680)}$, $D_{f_2(1270)}$, $D_{\omega(892)}$ and D_{DCS} . In total, we have 24 real parameters to determine. For comparison, the Babar model [66] for the $D^0 \rightarrow K_S\pi^-\pi^+$ amplitude involves 43 parameters, while the model used by Belle [69] involves 40. The model proposed in ref. [70], which assumes a structure based on naive factorisation, involves 33 free parameters. The parameters ξ which influence the values of the S -wave phases in the inelastic region are also tuned to improve the results. For πK we take $\xi_{\pi K} = 0.515$ for the F -functions and $\xi_{\pi K} = 0.5293$ for the H -functions, while for $\pi\pi$ we take $\xi_{\pi\pi} = 0.53025$. We have included only the results from

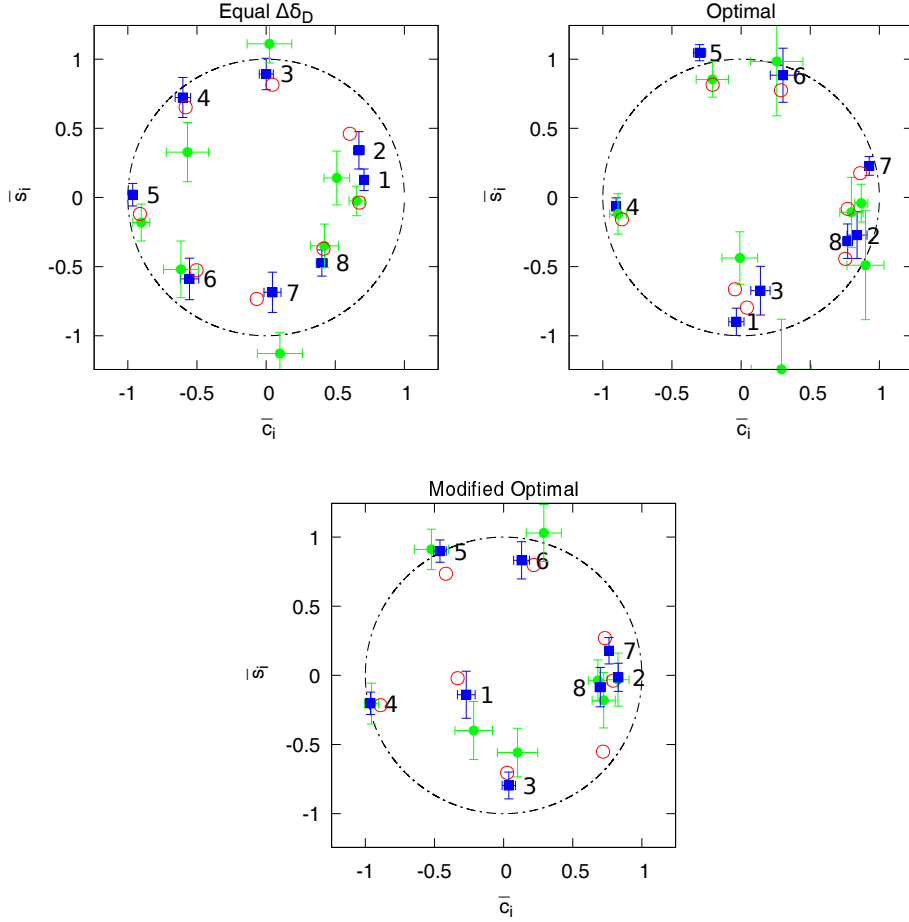


Figure 11: Experimental values of the cosine and sine averages \bar{c}_i, \bar{s}_i (ref. [30]: green circles, ref. [29]: blue squares) compared with the results from our amplitude (red circles).

the BESIII experiment [30] in the fit since they are compatible with the previous results from CLEO [29] and have significantly smaller statistical uncertainties. We perform a fit by minimising a χ^2 which includes:

- a) The 48 values F_i of the number of events in each bin i ,
- b) The 16 pairs of values \bar{c}_i, \bar{s}_i of the cosine and sine averages in the two binnings “Equal $\Delta\delta_D$ ” and “Modified Optimal”. The “Optimal” binning was not included in order not to give too much weight to these phase integrals and because one pair \bar{c}_i, \bar{s}_i fails to satisfy (4.37).

c) The 3 experimental values of the D^0 decay widths [36],

$$\begin{aligned}\Gamma_{D^0 \rightarrow K_S \pi^- \pi^+}^{exp} &= (4.49 \pm 0.29) \cdot 10^{-14} \text{ GeV} \\ \Gamma_{D^0 \rightarrow K^- \pi^0 \pi^+}^{exp} &= (23.10 \pm 0.80) \cdot 10^{-14} \text{ GeV} \\ \Gamma_{D^0 \rightarrow K_S \pi^0 \pi^0}^{exp} &= (1.46 \pm 0.18) \cdot 10^{-14} \text{ GeV} .\end{aligned}\tag{4.39}$$

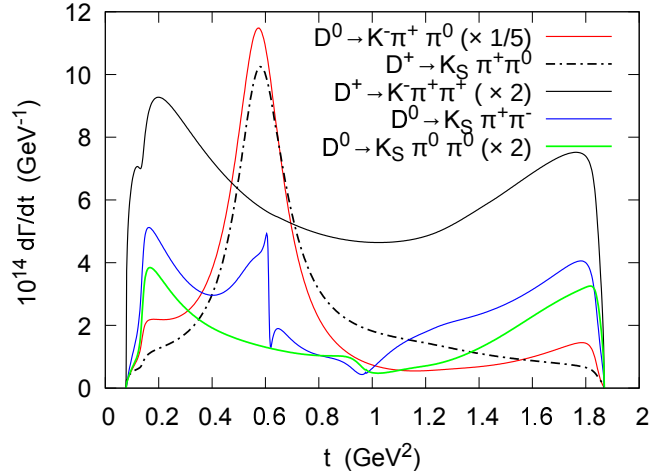


Figure 12: Distributions of the widths as a function of the $\pi\pi$ energy squared, $d\Gamma/dt$, for the various $D \rightarrow \bar{K}\pi\pi$ decay modes as predicted from isospin symmetry and our fits to the two modes $D^+ \rightarrow K_S \pi^0 \pi^+$ and $D^0 \rightarrow K_S \pi^- \pi^+$.

The input experimental data are described in a qualitatively correct, but not highly precise way, with a χ^2 per-point value $\chi^2/N = 1.99$. These results are illustrated in figs. 10 and 11 which show respectively the number of events F_i and the averages \bar{c}_i, \bar{s}_i . The agreement between the data and the model is best in the case of the “Equal $\Delta\delta_D$ ” binning. The fitted amplitude also reproduces the experimental values of the three D^0 widths (4.39) within their errors. The various $D \rightarrow \bar{K}\pi\pi$ widths show remarkable differences, e.g. the width of the $D^0 \rightarrow K^- \pi^0 \pi^+$ mode is 16 times larger than that of the $D^0 \rightarrow K_S \pi^0 \pi^0$ mode. These differences reflect the interference patterns of the one-variable amplitudes as encoded in eqs. (2.33)-(2.37). The reason for the large value of $\Gamma_{D^0 \rightarrow K^- \pi^0 \pi^+}$ is partly due to the fact that two $I = 1$ amplitudes add coherently in the combination $G_1^1 + 2 \tilde{G}_1^1$ which appears in the corresponding amplitude, generating a large $\rho(770)$ peak. This is illustrated in fig. 12 which shows the distribution $d\Gamma_{K^- \pi^0 \pi^+}/dt$ (divided by 5) compared to the other distributions. It is in qualitative agreement with the measurement by the CLEO collaboration [71]. The smallest width is that of the $D^0 \rightarrow K_S \pi^0 \pi^0$ mode which is four times smaller than the width of the mode $D^+ \rightarrow K^- \pi^+ \pi^+$. The main difference between these two amplitudes is a significant suppression

of the $I = 1/2$ S -wave in the former due to a cancellation in the combination $\sqrt{2}F_0^{1/2} - H_0^{1/2}$ which appears in eq. (2.37). The isobar-type model proposed in ref. [72] for the $K_S\pi^0\pi^0$ mode includes no $I = 1/2$ S -wave contribution at all, which is probably an oversimplification. The distribution $d\Gamma_{K_S\pi^0\pi^0}/dt$ (ignoring the DCS contribution as it cannot be deduced from isospin symmetry) is also shown in fig. 12. It is qualitatively similar to the CLEO measurement [72].

Parameter	Modulus		Phase(radians)
d_0	29.20 ± 4.25		-1.96 ± 0.16
d_1	42.10 ± 6.17	GeV^{-2}	1.07 ± 0.15
d_2	7.90 ± 1.03	GeV^{-4}	-1.58 ± 0.19
d_3	3.08 ± 0.09	GeV^{-4}	-1.36 ± 0.14
d_4	12.85 ± 3.35	GeV^{-4}	2.63 ± 0.24
d_5	6.49 ± 0.91	GeV^{-2}	-2.34 ± 0.15
d_6	12.80 ± 1.64	GeV^{-4}	0.98 ± 0.16
$D_{\omega(892)}$	0.12 ± 0.04	GeV^{-2}	-2.06 ± 0.36
$D_{K_2^*(1430)}$	0.13 ± 0.02	GeV^{-6}	-0.78 ± 0.21
$D_{K^*(1680)}$	5.41 ± 0.30	GeV^{-2}	0.17 ± 0.17
$D_{f_2(1270)}$	1.95 ± 0.11	GeV^{-4}	-2.69 ± 0.17
D_{DCS}	0.25 ± 0.03	GeV^{-2}	-1.33 ± 0.20

Table 2: Numerical parameters in the amplitude $D^0 \rightarrow K_S\pi^-\pi^+$ (see eq. (4.38)) resulting from the fit.

4.6 Comparison of the F - and H -functions

The magnitudes of the H -functions resulting from the fit (the numerical values of the corresponding parameters are given in table 2) are shown in fig. 8 (right). They can be compared to the magnitudes of the fitted F -functions which are shown in the same figure (left). The P -wave function $H_1^{1/2}$ is larger than the corresponding $F_1^{1/2}$ by a factor of four while the S -waves $F_0^{1/2}$, $H_0^{1/2}$ are roughly comparable in magnitude in the physical region but rather different in their shapes, in particular concerning the shapes of the cusps at the πK threshold. Fig. 13 compares the phases of the $F_0^{1/2}$ and $H_0^{1/2}$ functions. While the phase of $F_0^{1/2}$ increases steadily in the low energy region (in agreement with the phases determined through bin-by-bin measurements in refs. [63, 13, 64]⁹) the phase of $H_0^{1/2}$ is flat and slowly decreasing. Interestingly, these different behaviours in the

⁹The value $c_3 = -1$ (see table 1) for the parameter appearing in the P -wave amplitude $F_1^{1/2}$ was chosen such as to correspond to the normalisation of the $K^*(892)$ Breit-Wigner function in these references.

threshold region cannot be generated by the polynomial terms in the KT representation (since they are smooth functions). They must be caused by the rescattering integrals \widehat{I} which have a cusp at the πK threshold which combines with the cusp present in the Omnès function $\Omega_0^{1/2}$. This provides an interpretation to the fact that, within isobar model descriptions, a strong contribution from the broad κ resonance is required in D^+ amplitudes [10, 11, 13, 28] but not in D^0 amplitudes (e.g. [73]).

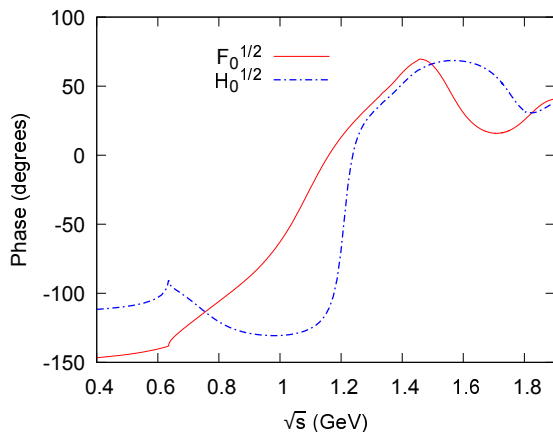


Figure 13: Comparison of the phases of the πK S -wave amplitudes $F_0^{1/2}$ and $H_0^{1/2}$.

A remark is in order, finally, concerning the DCS amplitude for which we have used a very crude description involving simply the $K^*(892)^+$ resonance. While the DCS amplitude is small (compared to the Cabibbo favoured one) it can significantly affect the phase of the overall amplitude. Previous fits [31, 66, 74] of the $K_S\pi^-\pi^+$ mode have included several additional contributions from $K_0^*(1430)^+$, $K_2^*(1430)^+$, $K^*(1680)^+$,... resonances. The DCS operator can also couple to states like $K^0\rho^0(770)$, $K^0f_0(980)$... which cannot be distinguished from $\bar{K}^0\rho^0(770)$, $\bar{K}^0f_0^0(980)$ unless measurements of both $K_S\pi^-\pi^+$ and $K_L\pi^-\pi^+$ are performed. We find clear indications that additional contributions are necessary since, with our crude DCS model, we cannot reproduce the experimental results of both the $K_S\pi^+\pi^-$ and the $K_L\pi^+\pi^-$ modes which are reported in refs. [29, 30] and we have thus focused only on the $K_S\pi^-\pi^+$ mode. As mentioned above in the case of the D^+ , making use of the isospin symmetry and inputs from a mode without DCS contributions (i.e. the $K^-\pi^0\pi^+$ mode) would allow a more complete determination of the DCS amplitude in the $K_S\pi^-\pi^+$ mode.

5 Conclusions

The main result of our work is contained in the formulas (2.33) to (2.37) which express all the $D \rightarrow \bar{K}\pi\pi$ amplitudes in terms of 6 F -functions plus 6 H -functions which

depend on one of the Mandelstam variables. These formulas derive from the fact that the relevant weak Hamiltonian for these decays is a pure isospin 1 operator and from the reconstruction theorem limited to $j = 0, 1$ partial-waves. The formulas apply to isobar-type models as well and, in that framework, can be easily generalised to contain $j \geq 2$ resonances. Based on this representation, we have derived two sets of coupled Khuri-Treiman equations, which generalise the previous results of refs. [21, 24]. Solving (numerically) these integral equations, the two sets of F - and H -functions get determined as linear combinations in terms of respectively 6 and 13 complex parameters.

In order to enlarge the region of applicability of the results two additional parameters are introduced which control the behaviour of the πK and $\pi\pi$ S -wave phases in the region where scattering is no longer elastic, allowing to simulate e.g. some cusp effects. As a check of this procedure, we have considered the soft pion relations which constrain the amplitudes at the two points $s, u = (m_K^2, m_D^2)$ and (m_D^2, m_K^2) and are sensitive to these parameters. A description of the complete Dalitz plot region requires further small contributions from higher spin or mass resonances and, eventually, from Cabibbo suppressed amplitudes: we describe these in a simple isobar-type model.

We have illustrated some applications of these results by performing a combined fit of a set of data for the $D^+ \rightarrow K_S \pi^0 \pi^+$ mode and a set of data for the $D^0 \rightarrow K_S \pi^- \pi^+$ mode. A rather good description of the D^+ data can be obtained in this manner, clearly showing the presence of the small DCS contribution. Concerning the D^0 , the available data refer to binnings with only eight bins. We have then used a limited number of parameters in particular in the description of the DCS amplitude. These data are nevertheless rather constraining as they concern the behaviour of both the modulus and the phase of the amplitude in these bins. The obtained $\chi^2/N \simeq 1.99$ is moderately good but the estimates of the H -functions seem already reasonable. This is illustrated in the result for the energy distributions of the widths, shown in fig. 12, which indicate correct interference patterns between the F and the H functions. An interesting difference between the two S -wave functions $F_0^{1/2}$ and $H_0^{1/2}$ can be observed near the threshold, see fig. 13 which shows the phases. This difference illustrates a clear three-body rescattering effect, which is accounted for in the KT formalism.

Our results allow one to introduce constraints in phenomenological models by performing combined fits of several D decay modes. Such fits have been performed in the past [75, 76, 77] without, however, making use of the isospin symmetry relations. The modes with a K_S (or a K_L) receive a small DCS contribution. Making use of isospin symmetry in the evaluation of the Cabibbo favoured component would enable one to determine this DCS part more completely than has been possible so far. As more data become available for DCS amplitudes [78, 79] one could also make use of isospin symmetry in this sector.

Acknowledgements: We would like to thank Prof. Chengdong Fu for send-

ing us the experimental results of the BESIII publication [28] and Prof. Andrzej Kupsc for his efficient help. We thank Prof. Jim Libby for correspondence and explanations and for sending us the lookup tables of the Babar model. This work is supported in part by the European Union's Horizon2020 research and innovation programme (HADRON-2020) under the grant agreement N° 824093.

A Soft pion limits

Application of the soft pion theorems (e.g. [80], chap. IV) to the $D \rightarrow \bar{K}\pi\pi$ amplitudes relates these to $D \rightarrow \bar{K}\pi$ amplitudes at the kinematical points $s, u = (m_D^2, m_K^2)$ or (m_K^2, m_D^2) which provides qualitative but interesting constraints on the scalar $\bar{K}\pi$ component of the $D \rightarrow \bar{K}\pi\pi$ amplitudes [81]. The soft pion relations have the following form

$$\lim_{p=0} \langle \bar{K}\pi^b\pi^a(p) | H_W(0) | D \rangle = -\frac{i}{F_\pi} \langle \bar{K}\pi^b | [Q_5^a, H_W(0)] | D \rangle \quad (\text{A.1})$$

(analogous to those for $K \rightarrow 3\pi$ [82]) where a, b are isospin indices, Q_5^a is an axial charge and $F_\pi \simeq 92.2$ MeV is the pion decay constant. Isospin symmetry allows one to express the three physical $D \rightarrow \bar{K}\pi$ amplitudes in terms of two isospin amplitudes $A^{1/2}$, $A^{3/2}$ [83],

$$\begin{aligned} A(D^+ \rightarrow \bar{K}^0\pi^+) &= A^{3/2} \\ A(D^0 \rightarrow K^-\pi^+) &= \frac{1}{3} (A^{3/2} + 2A^{1/2}) \\ A(D^0 \rightarrow \bar{K}^0\pi^0) &= \frac{\sqrt{2}}{3} (A^{3/2} - A^{1/2}) \end{aligned} \quad (\text{A.2})$$

and using the experimental results [36]

$$\begin{aligned} \Gamma(D^+ \rightarrow \bar{K}^0\pi^+) &= (1.93 \pm 0.04) \cdot 10^{-14}, \\ \Gamma(D^0 \rightarrow K^-\pi^+) &= (6.33 \pm 0.05) \cdot 10^{-14}, \\ \Gamma(D^0 \rightarrow \bar{K}^0\pi^0) &= (3.59 \pm 0.12) \cdot 10^{-14} \end{aligned} \quad (\text{A.3})$$

(all in GeV) one deduces from (A.2) the absolute values of the two isospin amplitudes

$$|A^{3/2}| = (1.40 \pm 0.01) 10^{-6} \text{ (GeV)}, \quad |A^{1/2}| = (3.76 \pm 0.03) 10^{-6} \text{ (GeV)} \quad (\text{A.4})$$

and the value of the phase difference

$$\phi^{1/2} - \phi^{3/2} = \pm(91.8 \pm 2.0)^\circ. \quad (\text{A.5})$$

Considering all the $D \rightarrow \bar{K}\pi_1\pi_2$ amplitudes, one can write three relations of the type (A.1) corresponding to a soft π^0 , four relations corresponding to a soft π^+ and one relation with a soft π^- . The latter relation is special because the combination

	$10^5 \frac{ A^{1/2} }{F_\pi}$	$10^5 \frac{ A^{3/2} }{F_\pi}$	$\phi^{1/2} - \phi^{3/2}$
Exp.	4.08(3)	1.52(1)	$\pm 91.8(2.0)^\circ$
$\xi = 0.515$	2.62	0.98	$+98.5^\circ$
$\xi = 0.5293$	3.99	1.29	-96.5°

Table 3: Test of the two soft pion relations (A.8) as a function of the parameter ξ which tunes the value of the πK phase in the inelastic region according to (4.1). For a given value of ξ , the polynomial parameters c_i are derived from a best fit to the data.

which appears on the right-hand side

$$\lim_{p=0} \langle \bar{K}^0 \pi^- (p) \pi^+ | H_W | D^0 \rangle = \frac{1}{\sqrt{2} F_\pi} \left(A(D^+ \rightarrow \bar{K}^0 \pi^+) - A(D^0 \rightarrow K^- \pi^+) - \sqrt{2} A(D^0 \rightarrow \bar{K}^0 \pi^0) \right) = 0 \quad (\text{A.6})$$

vanishes upon using the isospin relations (A.1). This corresponds to a zero of the amplitude $A_{\bar{K}^0 \pi^- \pi^+}$ at the point $s = m_K^2$, $u = m_D^2$. This is the only soft pion zero. For instance, for the same amplitude at the symmetric point $s = m_D^2$, $u = m_K^2$ one obtains

$$\lim_{p=0} \langle \bar{K}^0 \pi^- \pi^+ (p) | H_W | D^0 \rangle = \frac{i}{F_\pi} A(D^0 \rightarrow \bar{K}^0 \pi^0) . \quad (\text{A.7})$$

Only four (out of the eight) soft-pion relations are independent. One can first write two relations which involve only the F -functions

$$\begin{aligned} \frac{iA^{1/2}}{F_\pi} &= -3F_0^{1/2}(m_D^2) - 2F_0^{1/2}(m_K^2) - 5F_0^{3/2}(m_K^2) + \frac{5\sqrt{2}}{4}G_0^2(2m_\pi^2) - \Delta_{DK}G_1^1(2m_\pi^2) \\ \frac{iA^{3/2}}{F_\pi} &= 3F_0^{3/2}(m_D^2) - 2F_0^{3/2}(m_K^2) + F_0^{1/2}(m_K^2) - \frac{\sqrt{2}}{4}G_0^2(2m_\pi^2) - \Delta_{DK}G_1^1(2m_\pi^2) . \end{aligned} \quad (\text{A.8})$$

In writing these relations, we have dropped all contributions which are $O(m_\pi^2)$, in particular, those involving the angular factors Z_s, Z_u . The right-hand sides of the relations (A.8) are sensitive to the value of the parameter ξ which we introduced for tuning the $I = 1/2$ πK S -wave phase above the inelastic threshold. Table 3 illustrates that taking a value of the ξ parameter slightly larger than 0.5, the right orders of magnitudes can be obtained for the soft pion relations (A.8). It is possible to fine-tune the value of ξ such that they are satisfied within 15%. The last two independent soft pion relations

	$\mathcal{F}^{\frac{3}{2}\frac{3}{2}}$	$\mathcal{F}^{\frac{1}{2}\frac{3}{2}}$	$\mathcal{F}^{\frac{3}{2}\frac{1}{2}}$	$\mathcal{F}^{\frac{1}{2}\frac{1}{2}}$		\mathcal{G}^{10}	\mathcal{G}^{12}	\mathcal{G}^{01}	\mathcal{G}^{11}
\mathcal{A}_1	$-\frac{2\sqrt{2}}{3\sqrt{15}}$	$\frac{1}{3\sqrt{3}}$	$-\frac{\sqrt{2}}{3\sqrt{3}}$	$\frac{2\sqrt{2}}{3\sqrt{3}}$	$\tilde{\mathcal{A}}_1$	0	$\frac{\sqrt{3}}{\sqrt{5}}$	0	0
\mathcal{A}_2	$-\frac{4}{3\sqrt{15}}$	$\frac{2}{3\sqrt{6}}$	$+\frac{1}{3\sqrt{3}}$	$-\frac{2}{3\sqrt{3}}$	$\tilde{\mathcal{A}}_2$	0	$-\frac{\sqrt{3}}{2\sqrt{10}}$	$-\frac{1}{2\sqrt{3}}$	$+\frac{1}{2\sqrt{2}}$
\mathcal{A}_3	$\frac{2}{\sqrt{15}}$	$-\frac{1}{\sqrt{6}}$	0	0	$\tilde{\mathcal{A}}_3$	0	$-\frac{\sqrt{3}}{2\sqrt{10}}$	$+\frac{1}{2\sqrt{3}}$	$-\frac{1}{2\sqrt{2}}$
\mathcal{A}_4	$-\frac{2}{\sqrt{15}}$	0	$-\frac{1}{\sqrt{3}}$	0	$\tilde{\mathcal{A}}_4$	0	$\frac{\sqrt{3}}{2\sqrt{10}}$	$-\frac{1}{2\sqrt{3}}$	$-\frac{1}{2\sqrt{2}}$
\mathcal{A}_5	$\frac{4}{3\sqrt{15}}$	$+\frac{1}{3\sqrt{6}}$	$+\frac{2}{3\sqrt{3}}$	$+\frac{2}{3\sqrt{3}}$	$\tilde{\mathcal{A}}_5$	0	$\frac{\sqrt{3}}{2\sqrt{10}}$	$+\frac{1}{2\sqrt{3}}$	$+\frac{1}{2\sqrt{2}}$
\mathcal{A}_6	$\frac{\sqrt{2}}{\sqrt{15}}$	0	$-\frac{\sqrt{2}}{\sqrt{3}}$	0	$\tilde{\mathcal{A}}_6$	$\frac{1}{\sqrt{3}}$	$+\frac{1}{\sqrt{60}}$	0	$-\frac{1}{2}$
\mathcal{A}_7	$\frac{4\sqrt{2}}{3\sqrt{15}}$	$+\frac{1}{3\sqrt{3}}$	$-\frac{\sqrt{2}}{3\sqrt{3}}$	$-\frac{\sqrt{2}}{3\sqrt{3}}$	$\tilde{\mathcal{A}}_7$	$\frac{1}{\sqrt{3}}$	$-\frac{1}{\sqrt{15}}$	0	0
\mathcal{A}_8	$\frac{\sqrt{2}}{\sqrt{15}}$	$+\frac{1}{\sqrt{3}}$	0	0	$\tilde{\mathcal{A}}_8$	$\frac{1}{\sqrt{3}}$	$+\frac{1}{\sqrt{60}}$	0	$+\frac{1}{2}$

Table 4: Coefficients of the linear expansions of the physical amplitudes \mathcal{A}_i and $\tilde{\mathcal{A}}_i$ (defined in (B.1) (B.2)) in terms of isospin amplitudes.

can be written as

$$\begin{aligned}
H_0^{1/2}(m_D^2) &= -\sqrt{2} \left(F_0^{1/2}(m_D^2) + F_0^{1/2}(m_K^2) + \frac{4}{3}F_0^{3/2}(m_K^2) \right) + \frac{1}{3}H_0^{1/2}(m_K^2) \\
&\quad - \frac{8}{3}H_0^{3/2}(m_K^2) + \frac{10}{9}G_0^2(2m_\pi^2) - \frac{2}{3}G_0^0(2m_\pi^2) - \frac{4\sqrt{2}}{3}\Delta_{DK}\tilde{G}_1^1(2m_\pi^2) \\
H_0^{3/2}(m_D^2) &= \frac{\sqrt{2}}{3}F_0^{3/2}(m_K^2) - \frac{1}{3}H_0^{1/2}(m_K^2) - \frac{1}{3}H_0^{3/2}(m_K^2) \\
&\quad + \frac{1}{18}G_0^2(2m_\pi^2) - \frac{1}{3}G_0^0(2m_\pi^2) + \frac{\sqrt{2}}{3}\Delta_{DK}\tilde{G}_1^1(2m_\pi^2) .
\end{aligned} \tag{A.9}$$

Setting the value of ξ as in the last line of table 3 the first relation in eq. (A.9) is satisfied within $\simeq 50\%$, the left-hand side equalling $(8.6 + i5.9) 10^{-5}$ and the right-hand side: $(5.1 + i3.8) 10^{-5}$. The second relation fails to be satisfied even qualitatively. In that case, the left-hand side equals $(2.4 - i0.6) 10^{-6}$ and the right-hand side $(-9.8 + i1.8) 10^{-6}$, differing in their signs and by a factor of 4 in magnitude. This indicates that our evaluation of $H_0^{3/2}$ in the inelastic region is not quite correct. That relation on $H_0^{3/2}(m_D^2)$ also insures the presence of the zero in $A_{\bar{K}^0\pi^-\pi^+}$ at $s = m_K^2$, $u = m_D^2$ (see eq.(A.6)). Our solution amplitude is thus not sufficiently suppressed at this point.

B Details of the expansions with isospin amplitudes

B.1 General relations

Let us consider $2 \rightarrow 2$ scattering amplitudes induced by the weak Hamiltonian H_W : $\mathcal{A}(s, t, u) = \langle cd|H_W|ab \rangle$ with $s = (p_a + p_b)^2$, $t = (p_b - p_d)^2$, $u = (p_a - p_d)^2$. We start by forming 8 scattering amplitudes of the type $\langle D\pi_2|H_W|\bar{K}\pi_1 \rangle$ with all possible charges of

π_1, π_2 and \bar{K}

$$\begin{aligned}
\mathcal{A}_1 &= \langle D^+\pi^- | H_W | K^-\pi^+ \rangle & \mathcal{A}_5 &= \langle D^0\pi^0 | H_W | K^-\pi^+ \rangle \\
\mathcal{A}_2 &= \langle D^+\pi^- | H_W | \bar{K}^0\pi^0 \rangle & \mathcal{A}_6 &= \langle D^0\pi^- | H_W | \bar{K}^0\pi^- \rangle \\
\mathcal{A}_3 &= \langle D^+\pi^0 | H_W | \bar{K}^0\pi^+ \rangle & \mathcal{A}_7 &= \langle D^0\pi^0 | H_W | \bar{K}^0\pi^0 \rangle \\
\mathcal{A}_4 &= \langle D^0\pi^- | H_W | K^-\pi^0 \rangle & \mathcal{A}_8 &= \langle D^0\pi^+ | H_W | \bar{K}^0\pi^+ \rangle
\end{aligned} \tag{B.1}$$

and then 8 scattering amplitudes of the type $\langle DK | H_W | \pi_1\pi_2 \rangle$

$$\begin{aligned}
\tilde{\mathcal{A}}_1 &= \langle D^+K^+ | H_W | \pi^+\pi^+ \rangle & \tilde{\mathcal{A}}_5 &= \langle D^0K^+ | H_W | \pi^0\pi^+ \rangle \\
\tilde{\mathcal{A}}_2 &= \langle D^+K^0 | H_W | \pi^+\pi^0 \rangle & \tilde{\mathcal{A}}_6 &= \langle D^0K^0 | H_W | \pi^+\pi^- \rangle \\
\tilde{\mathcal{A}}_3 &= \langle D^+K^0 | H_W | \pi^0\pi^+ \rangle & \tilde{\mathcal{A}}_7 &= \langle D^0K^0 | H_W | \pi^0\pi^0 \rangle \\
\tilde{\mathcal{A}}_4 &= \langle D^0K^+ | H_W | \pi^+\pi^0 \rangle & \tilde{\mathcal{A}}_8 &= \langle D^0K^0 | H_W | \pi^-\pi^+ \rangle .
\end{aligned} \tag{B.2}$$

Next, using the following conventional isospin assignments

$$\begin{pmatrix} K^+ \\ K^0 \end{pmatrix} \sim \begin{pmatrix} |\frac{1}{2}\frac{1}{2}\rangle \\ |\frac{1}{2}\frac{-1}{2}\rangle \end{pmatrix}, \quad \begin{pmatrix} \bar{K}^0 \\ K^- \end{pmatrix} \sim \begin{pmatrix} |\frac{1}{2}\frac{1}{2}\rangle \\ -|\frac{1}{2}\frac{-1}{2}\rangle \end{pmatrix}, \quad \begin{pmatrix} D^+ \\ D^0 \end{pmatrix} \sim \begin{pmatrix} |\frac{1}{2}\frac{1}{2}\rangle \\ -|\frac{1}{2}\frac{-1}{2}\rangle \end{pmatrix} \tag{B.3}$$

and

$$\begin{pmatrix} \pi^+ \\ \pi^0 \\ \pi^- \end{pmatrix} \sim \begin{pmatrix} -|11\rangle \\ |10\rangle \\ |1,-1\rangle \end{pmatrix} \tag{B.4}$$

one can expand the two particle states in terms of isospin states and then apply the Wigner-Eckart theorem (2.19). The resulting coefficients of the expressions of the physical amplitudes \mathcal{A}_i in terms of the isospin amplitudes $\mathcal{F}^{KK'}$ and those of $\tilde{\mathcal{A}}_i$ in terms of $\mathcal{G}^{II'}$ (see (2.25)) are collected in table 4.

The expressions of the D^+ amplitudes can be further simplified if we assume that the effects of the $D\pi$ or DK interactions can be neglected in the energy region of interest. This allows us to combine amplitudes with different isospins of $D\pi$ or DK . In the channels $\langle D\pi_i | H_W | \bar{K}\pi_j \rangle$ we introduce the following linear combinations and keep a unique isospin label referring to the $K\pi$ system

$$\begin{pmatrix} \mathcal{F}^{3/2} \\ \mathcal{F}^{1/2} \\ \mathcal{H}^{3/2} \\ \mathcal{H}^{1/2} \end{pmatrix} \equiv \begin{pmatrix} \frac{2}{3\sqrt{15}} & -\frac{1}{3\sqrt{6}} & 0 & 0 \\ 0 & 0 & \frac{1}{3\sqrt{3}} & -\frac{2}{3\sqrt{3}} \\ -\frac{\sqrt{2}}{3\sqrt{15}} & -\frac{1}{3\sqrt{3}} & 0 & 0 \\ 0 & 0 & \frac{\sqrt{2}}{\sqrt{3}} & 0 \end{pmatrix} \begin{pmatrix} \mathcal{F}^{\frac{3}{2}\frac{3}{2}} \\ \mathcal{F}^{\frac{1}{2}\frac{3}{2}} \\ \mathcal{F}^{\frac{3}{2}\frac{1}{2}} \\ \mathcal{F}^{\frac{1}{2}\frac{1}{2}} \end{pmatrix}. \tag{B.5}$$

Similarly, in the channels $\langle DK | H_W | \pi_i\pi_j \rangle$ we introduce four combinations labelled with the isospin of the pion pair,

$$\begin{pmatrix} \mathcal{G}^0 \\ \mathcal{G}^2 \\ \mathcal{G}^1 \\ \tilde{\mathcal{G}}^1 \end{pmatrix} \equiv \begin{pmatrix} -\frac{1}{\sqrt{3}} & 0 & 0 & 0 \\ 0 & \frac{\sqrt{3}}{\sqrt{5}} & 0 & 0 \\ 0 & 0 & -\frac{1}{2\sqrt{3}} & \frac{1}{2\sqrt{2}} \\ 0 & 0 & 0 & \frac{1}{2\sqrt{2}} \end{pmatrix} \begin{pmatrix} \mathcal{G}^{10} \\ \mathcal{G}^{12} \\ \mathcal{G}^{01} \\ \mathcal{G}^{11} \end{pmatrix}. \tag{B.6}$$

	$\mathcal{F}^{3/2}$	$\mathcal{F}^{1/2}$	$\mathcal{H}^{3/2}$	$\mathcal{H}^{1/2}$		\mathcal{G}^0	\mathcal{G}^2	\mathcal{G}^1	$\tilde{\mathcal{G}}^1$
\mathcal{A}_1	$-\sqrt{2}$	$-\sqrt{2}$	0	0	$\tilde{\mathcal{A}}_1$	0	1	0	0
\mathcal{A}_2	-2	1	0	0	$\tilde{\mathcal{A}}_2$	0	$-\frac{\sqrt{2}}{4}$	1	0
\mathcal{A}_3	3	0	0	0	$\tilde{\mathcal{A}}_3$	0	$-\frac{\sqrt{2}}{4}$	-1	0
\mathcal{A}_4	-2	0	$\sqrt{2}$	$-\frac{1}{\sqrt{2}}$	$\tilde{\mathcal{A}}_4$	0	$-\frac{\sqrt{2}}{4}$	1	-2
\mathcal{A}_5	1	-1	$-\sqrt{2}$	$\frac{1}{\sqrt{2}}$	$\tilde{\mathcal{A}}_5$	0	$\frac{\sqrt{2}}{4}$	-1	2
\mathcal{A}_6	$\sqrt{2}$	0	-1	-1	$\tilde{\mathcal{A}}_6$	-1	$\frac{1}{6}$	0	$-\sqrt{2}$
\mathcal{A}_7	$\sqrt{2}$	$\frac{1}{\sqrt{2}}$	-2	$-\frac{1}{2}$	$\tilde{\mathcal{A}}_7$	-1	$-\frac{1}{3}$	0	0
\mathcal{A}_8	0	0	-3	0	$\tilde{\mathcal{A}}_8$	-1	$\frac{1}{6}$	0	$\sqrt{2}$

Table 5: Expansion coefficients of the physical amplitudes \mathcal{A}_i and $\tilde{\mathcal{A}}_i$ in terms of the new isospin amplitudes.

The coefficients of the expansions of the physical amplitudes in terms of these new isospin amplitudes are given in table 5. One notes, in particular, that the expansions of the D^+ amplitudes (first three lines in the tables) now involve only two isospin amplitudes instead of four.

B.2 Crossing symmetries

The amplitudes \mathcal{A}_i , $\tilde{\mathcal{A}}_i$ obey a number of crossing symmetry relations. Under $s - t$ crossing one has the 8 relations

$$\tilde{\mathcal{A}}_i(s, t, u) = \mathcal{A}_i(t, s, u) \quad (\text{B.7})$$

and under $s - u$ crossing one has 5 relations

$$\begin{aligned} \mathcal{A}_1(s, t, u) &= \mathcal{A}_1(u, t, s), \\ \mathcal{A}_2(s, t, u) &= \mathcal{A}_3(u, t, s), \\ \mathcal{A}_4(s, t, u) &= \mathcal{A}_5(u, t, s), \\ \mathcal{A}_6(s, t, u) &= \mathcal{A}_8(u, t, s), \\ \mathcal{A}_7(s, t, u) &= \mathcal{A}_7(u, t, s). \end{aligned} \quad (\text{B.8})$$

The crossing-symmetry relations (B.7) (B.8) induce corresponding linear relations among the isospin amplitudes. Collecting the isospin amplitudes into vectors $\vec{\mathcal{F}}(s, t, u)$ and $\vec{\mathcal{G}}(s, t, u)$ (see eq. (2.29)) one has the crossing relations given in eq. (2.30) in which the

crossing matrices \mathbf{C}_{st} , \mathbf{C}_{us} read

$$\mathbf{C}_{st} = \begin{pmatrix} -\frac{2\sqrt{2}}{3} & -\frac{\sqrt{2}}{6} & 2 & \frac{1}{2} \\ -\sqrt{2} & -\sqrt{2} & 0 & 0 \\ -\frac{5}{2} & \frac{1}{2} & 0 & 0 \\ -\frac{1}{2} & 0 & -\frac{\sqrt{2}}{2} & \frac{\sqrt{2}}{4} \end{pmatrix}, \quad \mathbf{C}_{us} = \begin{pmatrix} -\frac{2}{3} & \frac{1}{3} & 0 & 0 \\ \frac{5}{3} & \frac{2}{3} & 0 & 0 \\ -\frac{\sqrt{2}}{3} & 0 & \frac{1}{3} & \frac{1}{3} \\ -\frac{\sqrt{2}}{3} & \frac{\sqrt{2}}{3} & \frac{8}{3} & -\frac{1}{3} \\ . & . & . & . \end{pmatrix}. \quad (\text{B.9})$$

We note that they satisfy the following properties

$$\mathbf{C}_{us}^2 = \mathbf{1}, \quad \mathbf{C}_{st}\mathbf{C}_{us}\mathbf{C}_{st}^{-1} = \text{diag}(1, 1, -1, -1). \quad (\text{B.10})$$

With the ingredients presented above we can write the representation of the isospin amplitudes in terms of single-variable functions which derive from the reconstruction theorem [32]. Including $j = 0, 1$ partial-waves, we can collect the relevant one-variable functions into vectors \vec{F}_0 , \vec{F}_1 , \vec{G}_0 , \vec{G}_1 as given in eq. (2.31). Imposing the crossing-symmetry relations one finds that the representation with single-variable functions must have the form given in eq. (2.32). Using these relations together with table 5 one obtains the expressions of the physical amplitudes in terms of single-variable isospin amplitudes.

C Angular integrations

C.1 Hat-functions

We give below the expressions of the hat-functions in terms of angular integrals. For the z_s integrals we use the notation [84]

$$\begin{aligned} \langle z_s^n \Phi(u) \rangle_s &\equiv \frac{1}{2} \int_{-1}^1 dz_s z_s^n \Phi(u(s, z_s)) \\ \langle z_s^n \Phi(t) \rangle_s &\equiv \frac{1}{2} \int_{-1}^1 dz_s z_s^n \Phi(t(s, z_s)). \end{aligned} \quad (\text{C.1})$$

The hat-functions \widehat{F}_j^K have the following expressions

$$\begin{aligned}
\widehat{F}_0^{3/2}(s) &= -\frac{2}{3} \langle F_0^{3/2}(u) \rangle_s + \frac{1}{3} \langle F_0^{1/2}(u) \rangle_s - \frac{2}{3} \langle Z_u F_1^{3/2}(u) \rangle_s \\
&\quad + \frac{1}{3} \langle Z_u F_1^{1/2}(u) \rangle_s - \frac{\sqrt{2}}{12} \langle G_0^2(t) \rangle_s - \frac{1}{3} \langle Z_t G_1^1(t) \rangle_s \\
\widehat{F}_0^{1/2}(s) &= \frac{5}{3} \langle F_0^{3/2}(u) \rangle_s + \frac{2}{3} \langle F_0^{1/2}(u) \rangle_s + \frac{5}{3} \langle Z_u F_1^{3/2}(u) \rangle_s \\
&\quad + \frac{2}{3} \langle Z_u F_1^{1/2}(u) \rangle_s - \frac{5\sqrt{2}}{12} \langle G_0^2(t) \rangle_s + \frac{1}{3} \langle Z_t G_1^1(t) \rangle_s \\
\widehat{F}_1^{3/2}(s) &= \frac{1}{s\kappa_s(s)} \left[-2 \langle z_s F_0^{3/2}(u) \rangle_s + \langle z_s F_0^{1/2}(u) \rangle_s - 2 \langle z_s Z_u F_1^{3/2}(u) \rangle_s \right. \\
&\quad \left. + \langle z_s Z_u F_1^{1/2}(u) \rangle_s - \frac{1}{4} \sqrt{2} \langle z_s G_0^2(t) \rangle_s - \langle z_s Z_t G_1^1(t) \rangle_s \right] \\
\widehat{F}_1^{1/2}(s) &= \frac{1}{s\kappa_s(s)} \left[5 \langle z_s F_0^{3/2}(u) \rangle_s + 2 \langle z_s F_0^{1/2}(u) \rangle_s + 5 \langle z_s Z_u F_1^{3/2}(u) \rangle_s \right. \\
&\quad \left. + 2 \langle z_s Z_u F_1^{1/2}(u) \rangle_s - \frac{5}{4} \sqrt{2} \langle z_s G_0^2(t) \rangle_s + \langle z_s Z_t G_1^1(t) \rangle_s \right].
\end{aligned} \tag{C.2}$$

Where $Z_u \equiv -u(u + 2s - \Sigma) + \Delta$, $Z_t \equiv t + 2s - \Sigma$. Next, the hat-functions \widehat{H}_j^K read

$$\begin{aligned}
\widehat{H}_0^{3/2}(s) &= -\frac{\sqrt{2}}{3} \langle F_0^{3/2}(u) \rangle_s + \frac{1}{3} \langle H_0^{3/2}(u) \rangle_s + \frac{1}{3} \langle H_0^{1/2}(u) \rangle_s \\
&\quad - \frac{\sqrt{2}}{3} \langle Z_u F_1^{3/2}(u) \rangle_s + \frac{1}{3} \langle Z_u H_1^{3/2}(u) \rangle_s + \frac{1}{3} \langle Z_u H_1^{1/2}(u) \rangle_s \\
&\quad + \frac{1}{3} \langle G_0^0(t) \rangle_s - \frac{1}{18} \langle G_0^2(t) \rangle_s - \frac{\sqrt{2}}{3} \langle Z_t \widetilde{G}_1^1(t) \rangle_s \\
\widehat{H}_0^{1/2}(s) &= -\frac{\sqrt{2}}{3} \langle F_0^{3/2}(u) \rangle_s + \frac{\sqrt{2}}{3} \langle F_0^{1/2}(u) \rangle_s + \frac{8}{3} \langle H_0^{3/2}(u) \rangle_s - \frac{1}{3} \langle H_0^{1/2}(u) \rangle_s \\
&\quad - \frac{\sqrt{2}}{3} \langle Z_u F_1^{3/2}(u) \rangle_s + \frac{\sqrt{2}}{3} \langle Z_u F_1^{1/2}(u) \rangle_s \\
&\quad + \frac{8}{3} \langle Z_u H_1^{3/2}(u) \rangle_s - \frac{1}{3} \langle Z_u H_1^{1/2}(u) \rangle_s \\
&\quad + \frac{2}{3} \langle G_0^0(t) \rangle_s - \frac{5}{18} \langle G_0^2(t) \rangle_s - \frac{\sqrt{2}}{3} \langle Z_t G_1^1(t) \rangle_s + \frac{4\sqrt{2}}{3} \langle Z_t \widetilde{G}_1^1(t) \rangle_s \\
\widehat{H}_1^{3/2}(s) &= \frac{1}{s\kappa_s(s)} \left[-\sqrt{2} \langle z_s F_0^{3/2}(u) \rangle_s + \langle z_s H_0^{3/2}(u) \rangle_s + \langle z_s H_0^{1/2}(u) \rangle_s \right. \\
&\quad - \sqrt{2} \langle z_s Z_u F_1^{3/2}(u) \rangle_s + \langle z_s Z_u H_1^{3/2}(u) \rangle_s + \langle z_s Z_u H_1^{1/2}(u) \rangle_s \\
&\quad \left. + \langle z_s G_0^0(t) \rangle_s - \frac{1}{6} \langle z_s G_0^2(t) \rangle_s - \sqrt{2} \langle z_s Z_t \widetilde{G}_1^1(t) \rangle_s \right] \\
\widehat{H}_1^{1/2}(s) &= \frac{1}{s\kappa_s(s)} \left[-\sqrt{2} \langle z_s F_0^{3/2}(u) \rangle_s + \sqrt{2} \langle z_s F_0^{1/2}(u) \rangle_s + 8 \langle z_s H_0^{3/2}(u) \rangle_s \right. \\
&\quad - \langle z_s H_0^{1/2}(u) \rangle_s - \sqrt{2} \langle z_s Z_u F_1^{3/2}(u) \rangle_s + \sqrt{2} \langle z_s Z_u F_1^{1/2}(u) \rangle_s \\
&\quad + 8 \langle z_s Z_u H_1^{3/2}(u) \rangle_s - \langle z_s Z_u H_1^{1/2}(u) \rangle_s + 2 \langle z_s G_0^0(t) \rangle_s \\
&\quad \left. - \frac{5}{6} \langle z_s G_0^2(t) \rangle_s - \sqrt{2} \langle z_s Z_t G_1^1(t) \rangle_s + 4 \sqrt{2} \langle z_s Z_t \widetilde{G}_1^1(t) \rangle_s \right].
\end{aligned} \tag{C.3}$$

Concerning the t -channel hat-functions, we will use the notation

$$\langle z_t^n \Phi(s) \rangle_t \equiv \frac{1}{2} \int_{-1}^1 dz_t z_t^n \Phi(s(t, z_t)) . \quad (\text{C.4})$$

The analogous integrals involving $\Phi(u)$ can be replaced using the relation,

$$\langle z_t^n \Phi(u) \rangle_t = (-1)^n \langle z_t^n \Phi(s) \rangle_t . \quad (\text{C.5})$$

The hat-functions $\widehat{G}_0^2, \widehat{G}_1^1(t)$ are given by

$$\begin{aligned} \widehat{G}_0^2(t) &= -2\sqrt{2} \langle F_0^{3/2}(s) \rangle_t - 2\sqrt{2} \langle F_0^{1/2}(s) \rangle_t \\ &\quad - 2\sqrt{2} \langle Z_s F_1^{3/2}(s) \rangle_t - 2\sqrt{2} \langle Z_s F_1^{1/2}(s) \rangle_t \\ \widehat{G}_1^1(t) &= \frac{1}{\kappa_t(t)} \left[-15 \langle z_t F_0^{3/2}(s) \rangle_t + 3 \langle z_t F_0^{1/2}(s) \rangle_t \right. \\ &\quad \left. - 15 \langle z_t Z_s F_1^{3/2}(s) \rangle_t + 3 \langle z_t Z_s F_1^{1/2}(s) \rangle_t \right] \end{aligned} \quad (\text{C.6})$$

where $Z_s = s(s + 2t - \Sigma) + \Delta$. The hat-functions $\widehat{G}_0^0, \widehat{G}_1^1$, finally, are given by

$$\begin{aligned} \widehat{G}_0^0(t) &= -\frac{4\sqrt{2}}{3} \langle F_0^{3/2}(s) \rangle_t - \frac{\sqrt{2}}{3} \langle F_0^{1/2}(s) \rangle_t + 4 \langle H_0^{3/2}(s) \rangle_t + \langle H_0^{1/2}(s) \rangle_t \\ &\quad - \frac{4\sqrt{2}}{3} \langle Z_s F_1^{3/2}(s) \rangle_t - \frac{\sqrt{2}}{3} \langle Z_s F_1^{1/2}(s) \rangle_t \\ &\quad + 4 \langle Z_s H_1^{3/2}(s) \rangle_t + \langle Z_s H_1^{1/2}(s) \rangle_t \\ \widehat{G}_1^1(t) &= \frac{1}{\kappa_t(t)} \left[-3 \langle z_t F_0^{3/2}(s) \rangle_t - 3\sqrt{2} \langle z_t H_0^{3/2}(s) \rangle_t + \frac{3}{2} \sqrt{2} \langle z_t H_0^{1/2}(s) \rangle_t \right. \\ &\quad \left. - 3 \langle z_t Z_s F_1^{3/2}(s) \rangle_t - 3\sqrt{2} \langle z_t Z_s H_1^{3/2}(s) \rangle_t + \frac{3}{2} \sqrt{2} \langle z_t Z_s H_1^{1/2}(s) \rangle_t \right] . \end{aligned} \quad (\text{C.7})$$

C.2 Angular integrals expressed in terms of kernels

The one-variable functions satisfy ordinary dispersion relations. We will use these in order to re-express the angular integrations over z_s and z_t . The dispersion relations are written below, taking into account the assumed asymptotic behaviour. Firstly, one has

$$\begin{aligned} F_0^{1/2}(w) &= c_0 + c_1' w + \frac{w^2}{\pi} \int_{(m_K+m_\pi)^2}^{\infty} \frac{\text{disc}[F_0^{1/2}(w')]}{(w')^2(w'-w)} dw' \\ F_0^{3/2}(w) &= \frac{w^2}{\pi} \int_{(m_K+m_\pi)^2}^{\infty} \frac{\text{disc}[F_0^{3/2}(w')]}{(w')^2(w'-w)} dw' \\ F_1^{1/2}(w) &= \frac{1}{\pi} \int_{(m_K+m_\pi)^2}^{\infty} \frac{\text{disc}[F_1^{1/2}(w')]}{(w'-w)} dw' \end{aligned}$$

$$\begin{aligned}
F_1^{3/2}(w) &= \frac{1}{\pi} \int_{(m_K+m_\pi)^2}^{\infty} \frac{\text{disc}[F_1^{3/2}(w')]}{(w'-w)} dw' \\
G_0^2(t) &= \frac{t^2}{\pi} \int_{4m_\pi^2}^{\infty} \frac{\text{disc}[G_0^2(t')]}{(t')^2(t'-t)} dt' \\
G_1^1(t) &= c_4 + \frac{t}{\pi} \int_{4m_\pi^2}^{\infty} \frac{\text{disc}[G_1^1(t')]}{(t')(t'-t)} dt'
\end{aligned} \tag{C.8}$$

with

$$c'_1 = c_1 + c_0 \dot{\Omega}_0^{1/2}(0) \tag{C.9}$$

and the remaining set reads

$$\begin{aligned}
H_0^{1/2}(w) &= d_0 + d'_1 w + \frac{w^2}{\pi} \int_{(m_K+m_\pi)^2}^{\infty} \frac{\text{disc}[H_0^{1/2}(w')]}{(w')^2(w'-w)} dw' \\
H_0^{3/2}(w) &= \frac{w^2}{\pi} \int_{(m_K+m_\pi)^2}^{\infty} \frac{\text{disc}[H_0^{3/2}(w')]}{(w')^2(w'-w)} dw' \\
H_1^{1/2}(w) &= \frac{1}{\pi} \int_{(m_K+m_\pi)^2}^{\infty} \frac{\text{disc}[H_1^{1/2}(w')]}{(w'-w)} dw' \\
H_1^{3/2}(w) &= \frac{1}{\pi} \int_{(m_K+m_\pi)^2}^{\infty} \frac{\text{disc}[H_1^{3/2}(w')]}{(w'-w)} dw' \\
G_0^0(t) &= \frac{t^2}{\pi} \int_{4m_\pi^2}^{\infty} \frac{\text{disc}[G_0^0(t')]}{(t')^2(t'-t)} dt' \\
\tilde{G}_1^1(t) &= d_5 + \frac{t}{\pi} \int_{4m_\pi^2}^{\infty} \frac{\text{disc}[\tilde{G}_1^1(t')]}{(t')(t'-t)} dt'
\end{aligned} \tag{C.10}$$

with

$$d'_1 = d_1 + d_0 \dot{\Omega}_0^{1/2}(0) . \tag{C.11}$$

Computing angular integrals using eqs. (C.8) (C.10) one can invert the integrations order and perform the z_s, z_t integrations first, obtaining a set of kernels. These can be written in analytical form and encode the contour prescriptions for performing the angular integrals. Representations of the angular averages are then derived involving integrals of these kernels multiplied by discontinuities of the one-variable functions. For the F -functions, the z_s angular integrals can be expressed as follows

$$\begin{aligned}
\langle F_0^K(u) \rangle_s &= \delta_{2K,1} \left[c_0 + \frac{1}{2} c'_1 \left(\Sigma - s + \frac{\Delta}{s} \right) \right] - \frac{1}{\pi} \int_{(m_K+m_\pi)^2}^{\infty} K_u^0(s, u') \text{disc}[F_0^K(u')] du' \\
\langle z_s F_0^K(u) \rangle_s &= \delta_{2K,1} \left[-\frac{1}{6} c'_1 \kappa_s(s) \right] - \frac{1}{\pi} \int_{(m_K+m_\pi)^2}^{\infty} K_u^1(s, u') \text{disc}[F_0^K(u')] du'
\end{aligned}$$

$$\begin{aligned}
\langle Z_u F_1^K(u) \rangle_s &= \frac{-1}{\pi} \int_{(m_K+m_\pi)^2}^{\infty} K_{Z_u}^0(s, u') \text{disc}[F_1^K(u')] du' \\
\langle z_s Z_u F_1^K(u) \rangle_s &= \frac{-1}{\pi} \int_{(m_K+m_\pi)^2}^{\infty} K_{Z_u}^1(s, u') \text{disc}[F_1^K(u')] du' \\
\langle G_0^2(t) \rangle_s &= \frac{-1}{\pi} \int_{4m_\pi^2}^{\infty} K_t^0(s, t') \text{disc}[G_0^2(t')] dt' \\
\langle z_s G_0^2(t) \rangle_s &= \frac{-1}{\pi} \int_{4m_\pi^2}^{\infty} K_t^1(s, t') \text{disc}[G_0^2(t')] dt' \\
\langle Z_t G_1^1(t) \rangle_s &= c_4 \frac{1}{2} (3s - \Sigma - \frac{\Delta}{s}) - \frac{1}{\pi} \int_{4m_\pi^2}^{\infty} K_{Z_t}^0(s, t') \text{disc}[G_1^1(t')] dt' \\
\langle z_s Z_t G_1^1(t) \rangle_s &= c_4 \frac{1}{6} \kappa_s(s) - \frac{1}{\pi} \int_{4m_\pi^2}^{\infty} K_{Z_t}^1(s, t') \text{disc}[G_1^1(t')] dt' .
\end{aligned} \tag{C.12}$$

The representation of z_s integrals of the functions H_j^K and G_0^0 are analogous to those of F_j^K and G_0^2 respectively, eventually replacing the polynomial parameters c_i by d_i . The representation for \tilde{G}_1^1 is analogous to that of G_1^1 replacing the constant c_4 by d_4 . We express in a similar way the z_t angular integrals

$$\begin{aligned}
\langle F_0^K(s) \rangle_t &= \delta_{2K,1} [c_0 + \frac{1}{2} c_1' (\Sigma - t)] - \frac{1}{\pi} \int_{(m_K+m_\pi)^2}^{\infty} K_s^0(t, s') \text{disc}[F_0^K(s')] ds' \\
\langle z_t F_0^K(s) \rangle_t &= \delta_{2K,1} [\frac{1}{6} c_1' \kappa_t(t)] - \frac{1}{\pi} \int_{(m_K+m_\pi)^2}^{\infty} K_s^1(t, s') \text{disc}[F_0^K(s')] ds' \\
\langle Z_s F_1^K(s) \rangle_t &= \frac{-1}{\pi} \int_{(m_K+m_\pi)^2}^{\infty} K_{Z_s}^0(t, s') \text{disc}[F_1^K(s')] ds' \\
\langle z_t Z_s F_1^K(s) \rangle_t &= \frac{-1}{\pi} \int_{(m_K+m_\pi)^2}^{\infty} K_{Z_s}^1(t, s') \text{disc}[F_1^K(s')] ds' .
\end{aligned} \tag{C.13}$$

The twelve kernels which appear in eqs. (C.12), (C.13) can be written as follows, after making a change of variables

$$\begin{aligned}
K_u^0(s, u') &= \frac{1}{\kappa_s(s)} \int_{u_-(s)}^{u_+(s)} \frac{z^2}{(u')^2(z-u')} dz \\
K_u^1(s, u') &= \frac{1}{\kappa_s^2(s)} \int_{u_-(s)}^{u_+(s)} \frac{z^2(-2z + u_+(s) + u_-(s))}{(u')^2(z-u')} dz \\
K_{Z_u}^0(s, u') &= \frac{1}{\kappa_s(s)} \int_{u_-(s)}^{u_+(s)} \frac{-z^2 + z(\Sigma - 2s) + \Delta}{z-u'} dz \\
K_{Z_u}^1(s, u') &= \frac{1}{\kappa_s^2(s)} \int_{u_-(s)}^{u_+(s)} \frac{(-2z + u_+(s) + u_-(s))(-z^2 + z(\Sigma - 2s) + \Delta)}{z-u'} dz
\end{aligned}$$

$$\begin{aligned}
K_t^0(s, t') &= \frac{1}{\kappa_s(s)} \int_{t_-(s)}^{t_+(s)} \frac{z^2}{(t')^2(z-t')} dz \\
K_t^1(s, t') &= \frac{1}{\kappa_s^2(s)} \int_{t_-(s)}^{t_+(s)} \frac{z^2(2z-t_+(s)-t_-(s))}{(t')^2(z-t')} dz \\
K_{Z_t}^0(s, t') &= \frac{1}{\kappa_s(s)} \int_{t_-(s)}^{t_+(s)} \frac{z(z+2s-\Sigma)}{t'(z-t')} dz \\
K_{Z_t}^1(s, t') &= \frac{1}{\kappa_s^2(s)} \int_{t_-(s)}^{t_+(s)} \frac{z(z+2s-\Sigma)(2z-t_+(s)-t_-(s))}{t'(z-t')} dz \\
K_s^0(t, s') &= \frac{1}{\kappa_t(t)} \int_{s_-(t)}^{s_+(t)} \frac{z^2}{(s')^2(z-s')} dz \\
K_s^1(t, s') &= \frac{1}{\kappa_t^2(t)} \int_{s_-(t)}^{s_+(t)} \frac{z^2(2z-s_+(t)-s_-(t))}{(s')^2(z-s')} dz \\
K_{Z_s}^0(t, s') &= \frac{1}{\kappa_t(t)} \int_{s_-(t)}^{s_+(t)} \frac{(z^2+z(2t-\Sigma)+\Delta)}{z-s'} dz \\
K_{Z_s}^1(t, s') &= \frac{1}{\kappa_t^2(t)} \int_{s_-(t)}^{s_+(t)} \frac{(z^2+z(2t-\Sigma)+\Delta)(2z-s_+(t)-s_-(t))}{z-s'} dz \tag{C.14}
\end{aligned}$$

where

$$u_{\pm}(s) = \frac{1}{2}(\Sigma - s + \frac{\Delta}{s} \pm \kappa_s(s)), \quad t_{\pm}(s) = \frac{1}{2}(\Sigma - s - \frac{\Delta}{s} \pm \kappa_s(s)), \tag{C.15}$$

and

$$s_{\pm}(t) = \frac{1}{2}(\Sigma - t \pm \kappa_t(t)) . \tag{C.16}$$

When these integration endpoints are real and overlapping with the unitarity cut, they must be shifted infinitesimally from the real axis by using the prescription $m_D^2 \rightarrow m_D^2 + i\epsilon$. The twelve kernels (C.14) can easily be expressed in terms of three basic logarithms,

$$L_u(s, u') = \int_{u_-(s)}^{u_+(s)} \frac{dz}{z-u'}, \quad L_t(s, t') = \int_{t_-(s)}^{t_+(s)} \frac{dz}{z-t'}, \tag{C.17}$$

and

$$L_s(t, s') = \int_{s_-(t)}^{s_+(t)} \frac{dz}{z-s'} \tag{C.18}$$

which can be written in the following simple way in terms of the usual complex log function

$$\begin{aligned}
L_u(s, u') &= \log(u' - u_+(s)) - \log(u' - u_-(s)) \\
L_t(s, t') &= \log(t' - t_+(s)) - \log(t' - t_-(s)) \\
L_s(t, s') &= \log(s' - s_+(t)) - \log(s' - s_-(t)) . \tag{C.19}
\end{aligned}$$

The angular averages have singularities on the real axis when the variable s approaches $(m_D - m_\pi)^2$ (or the variable t approaches $(m_D - m_K)^2$) (e.g. [33]). Let us illustrate how these appear via the log functions. Consider, for instance, the kernel $K_u^0(s, u')$ (see (C.14)) whose expression is

$$K_u^0(s, u') = \frac{u' + u_+(s) + u_-(s)}{(u')^2} + \frac{L_u(s, u')}{\kappa_s(s)}. \quad (\text{C.20})$$

When $s \rightarrow (m_D - m_\pi)^2$ the function $\kappa_s(s)$ in the denominator vanishes while in the numerator $L_u(s, u')$ remains finite for a range of values of u'

$$(m_K + m_\pi)^2 \leq u' \leq u_\pm((m_D - m_\pi)^2) : L_u(s, u')|_{s \rightarrow (m_D - m_\pi)^2} = -2i\pi. \quad (\text{C.21})$$

This is because the integration boundaries $u_\pm(s)$ have equal real parts but opposite infinitesimal imaginary parts when $s \rightarrow (m_D - m_\pi)^2$. The divergence which is induced, for instance, in the angular average $\langle F_0^K(u) \rangle_s$ reads

$$\langle F_0^K(u) \rangle_s \Big|_{s \rightarrow (m_D - m_\pi)^2}^{\text{div}} = \frac{A}{\sqrt{((m_D - m_\pi)^2 - s)}} \int_{(m_K + m_\pi)^2}^{u_+((m_D - m_\pi)^2)} \text{disc}[F_0^K(u')] du' \quad (\text{C.22})$$

with $A = (m_D - m_\pi)^2 / \sqrt{m_D m_\pi \lambda_{K\pi}((m_D - m_\pi)^2)}$.

C.3 Breit-Wigner functions

We have used the following form for the Breit-Wigner functions used for describing some of the resonance contributions with $J = 1$ or $J = 2$

$$BW_J(w) = \frac{1}{m_r^2 - w - im_r \Gamma_r^J(w, \mu_1, \mu_2)} F_r^J(w, m_1, m_2) \quad (\text{C.23})$$

where m_r is the mass of the resonance. The energy dependence of the width assumes the dominance of a two-particle decay mode with masses μ_1, μ_2 ,

$$\Gamma_r^J(w, \mu_1, \mu_2) = \Gamma_r \times \left(\frac{q(w, \mu_1, \mu_2)}{q(m_r^2, \mu_1, \mu_2)} \right)^{2J+1} \frac{m_r}{\sqrt{w}} (F_r^J(w, \mu_1, \mu_2))^2 \quad (\text{C.24})$$

where q is the centre-of-mass momentum

$$q(w, \mu_1, \mu_2) = \sqrt{\frac{(w - (\mu_1 - \mu_2)^2)(w - (\mu_1 + \mu_2)^2)}{4w}} \quad (\text{C.25})$$

and F_r^J is a Blatt-Weisskopf penetration factor [85],

$$F_r^J(w, \mu_1, \mu_2) = \sqrt{\frac{1 + X_r^2}{1 + X^2}}, \quad F_r^2(w, \mu_1, \mu_2) = \sqrt{\frac{9 + 3X_r^2 + X_r^4}{9 + 3X^2 + X^4}} \quad (\text{C.26})$$

	$K^*(892)$	$K^*(1680)$	$K_2^*(1430)$	$\omega(782)$	$f_2(1270)$
m_r (MeV)	895.55	1718.0	1432.4	782.66	1275.5
Γ_r (MeV)	47.33	422.0	109.0	8.68	186.7

Table 6: Masses and widths parameters used in the Breit-Wigner functions. They correspond to the central values in the PDG except for the $K^*(1680)$ width which is taken at the upper end of the allowed values.

with $X = q(w, \mu_1, \mu_2)R$, $X_r = q(m_r^2, \mu_1, \mu_2)R$ and the value of the radius is taken as $R = 1.5 \text{ GeV}^{-1}$ (following [10]). A Blatt-Weisskopf factor is also included in eq. (C.23) corresponding to the vertex between the resonance and the two light pseudoscalar mesons. The values of the masses μ_1, μ_2 in eq. (C.24) are taken as $\mu_1 = m_\pi$ and $\mu_2 = m_\pi$ ($= m_K$) for a non-strange (strange) resonance except for the $K^*(1680)$ for which we choose $\mu_2 = m_{K^*(892)}$. In the case of $\omega(782)$ the width was taken as constant. The values of the masses and widths parameters m_r, Γ_r are collected in table 6.

References

- [1] **Belle-II** Collaboration, W. Altmannshofer *et. al.*, *The Belle II Physics Book*, *PTEP* **2019** (2019), no. 12 123C01, [[1808.10567](#)]. [Erratum: *PTEP* 2020, 029201 (2020)].
- [2] J. Kambor, J. H. Missimer, and D. Wyler, $K \rightarrow 2\pi$ and $K \rightarrow 3\pi$ decays in next-to-leading order chiral perturbation theory, *Phys. Lett.* **B261** (1991) 496–503.
- [3] J. Bijnens, P. Dhonte, and F. Borg, $K \rightarrow 3\pi$ decays in chiral perturbation theory, *Nucl. Phys. B* **648** (2003) 317–344, [[hep-ph/0205341](#)].
- [4] K. Kampf, M. Knecht, J. Novotný, and M. Zdráhal, *Dispersive construction of two-loop $P \rightarrow \pi\pi\pi$ ($P = K, \eta$) amplitudes*, *Phys. Rev. D* **101** (2020) 074043, [[1911.11762](#)].
- [5] S. Kränkl, T. Mannel, and J. Virto, *Three-body non-leptonic B decays and QCD factorization*, *Nucl. Phys. B* **899** (2015) 247–264, [[1505.04111](#)].
- [6] A. Bondar, *Improved Gronau-Wyler method for ϕ_3 extraction*, in *BINP Special Analysis Meeting on Dalitz Analysis, 24-26 Sept. 2002*, 2002.
- [7] A. Giri, Y. Grossman, A. Soffer, and J. Zupan, *Determining γ using $B^\pm \rightarrow DK^\pm$ with multibody D decays*, *Phys. Rev. D* **68** (2003) 054018, [[hep-ph/0303187](#)].

- [8] A. Bondar and A. Poluektov, *Feasibility study of model-independent approach to ϕ_3 measurement using Dalitz plot analysis*, *Eur. Phys. J. C* **47** (2006) 347–353, [[hep-ph/0510246](#)].
- [9] **CLEO** Collaboration, D. M. Asner *et. al.*, *Search for D^0 - anti- D^0 mixing in the Dalitz plot analysis of $D^0 \rightarrow K^0(S) \pi^+ \pi^-$* , *Phys. Rev. D* **72** (2005) 012001, [[hep-ex/0503045](#)].
- [10] **E791** Collaboration, E. M. Aitala *et. al.*, *Dalitz Plot Analysis of the Decay $D^+ \rightarrow K^- \pi^+ \pi^+$ and Indication of a Low-Mass Scalar $K\pi$ Resonance*, *Phys. Rev. Lett.* **89** (2002) 121801, [[hep-ex/0204018](#)].
- [11] **FOCUS** Collaboration, J. M. Link *et. al.*, *Dalitz plot analysis of the $D^+ \rightarrow K^- \pi^+ \pi^+$ decay in the FOCUS experiment*, *Phys. Lett. B* **653** (2007) 1–11, [[0705.2248](#)].
- [12] L. Edera and M. R. Pennington, *Estimating the $I = 3/2$ $K\pi$ interaction in D decay*, *Phys. Lett. B* **623** (2005) 55–64, [[hep-ph/0506117](#)].
- [13] **CLEO** Collaboration, G. Bonvicini *et. al.*, *Dalitz plot analysis of the $D^+ \rightarrow K^- \pi^+ \pi^+$ decay*, *Phys. Rev. D* **78** (2008) 052001, [[0802.4214](#)].
- [14] M. Diakonou and F. Diakonou, *The $K^- \pi^+ \pi^+$ Decay of the D^+ Meson*, *Phys. Lett. B* **216** (1989) 436–441.
- [15] J. A. Oller, *Final state interactions in hadronic D decays*, *Phys. Rev. D* **71** (2005) 054030, [[hep-ph/0411105](#)].
- [16] D. R. Boito, P. C. Magalhaes, M. R. Robilotta, and G. R. S. Zarnauskas, *Decay $D^+ \rightarrow K^- \pi^+ \pi^+$: Chiral symmetry and scalar resonances*, [0805.4803](#).
- [17] D. R. Boito and R. Escribano, *$K\pi$ form-factors and final state interactions in $D^+ \rightarrow K^- \pi^+ \pi^+$ decays*, *Phys. Rev. D* **80** (2009) 054007, [[0907.0189](#)].
- [18] P. C. Magalhães, M. R. Robilotta, K. S. F. F. Guimaraes, T. Frederico, W. de Paula, I. Bediaga, A. C. d. Reis, C. M. Maekawa, and G. R. S. Zarnauskas, *Towards three-body unitarity in $D^+ \rightarrow K^- \pi^+ \pi^+$* , *Phys. Rev. D* **84** (2011) 094001, [[1105.5120](#)].
- [19] K. S. F. F. Guimarães, O. Lourenço, W. de Paula, T. Frederico, and A. C. dos Reis, *Final state interaction in $D^+ \rightarrow K^- \pi^+ \pi^+$ with $K\pi$ $I = 1/2$ and $3/2$ channels*, *JHEP* **08** (2014) 135, [[1404.3797](#)].
- [20] S. X. Nakamura, *Coupled-channel analysis of $D^+ \rightarrow K^- \pi^+ \pi^+$ decay*, *Phys. Rev. D* **93** (2016) 014005, [[1504.02557](#)].

- [21] F. Niecknig and B. Kubis, *Dispersion-theoretical analysis of the $D^+ \rightarrow K^- \pi^+ \pi^+$ Dalitz plot*, *JHEP* **10** (2015) 142, [[1509.03188](#)].
- [22] C. Zemach, *Three pion decays of unstable particles*, *Phys. Rev.* **133** (1964) B1201.
- [23] T. J. Devlin and J. O. Dickey, *Weak Hadronic Decays: $K \rightarrow 2\pi$ and $K \rightarrow 3\pi$* , *Rev. Mod. Phys.* **51** (1979) 237.
- [24] F. Niecknig and B. Kubis, *Consistent Dalitz plot analysis of Cabibbo-favored $D^+ \rightarrow \bar{K} \pi \pi^+$ decays*, *Phys. Lett. B* **780** (2018) 471–478, [[1708.00446](#)].
- [25] N. Khuri and S. Treiman, *Pion-Pion Scattering and $K^\pm \rightarrow 3\pi$ Decay*, *Phys. Rev.* **119** (1960) 1115–1121.
- [26] R. F. Sawyer and K. C. Wali, *Pion-Pion Interactions in τ and τ' Decays*, *Phys. Rev.* **119** (1960) 1429–1435.
- [27] I. I. Y. Bigi and H. Yamamoto, *Interference between Cabibbo allowed and doubly forbidden transitions in $D \rightarrow K_{S,L} + \pi$'s decays*, *Phys. Lett. B* **349** (1995) 363–366, [[hep-ph/9502238](#)].
- [28] **BESIII** Collaboration, M. Ablikim *et. al.*, *Amplitude Analysis of the $D^+ \rightarrow K_S^0 \pi^+ \pi^0$ Dalitz Plot*, *Phys. Rev. D* **89** (2014) 052001, [[1401.3083](#)].
- [29] **CLEO** Collaboration, J. Libby *et. al.*, *Model-independent determination of the strong-phase difference between D^0 and $\bar{D}^0 \rightarrow K_{S,L}^0 h^+ h^-$ ($h = \pi, K$) and its impact on the measurement of the CKM angle γ/ϕ_3* , *Phys. Rev. D* **82** (2010) 112006, [[1010.2817](#)].
- [30] **BESIII** Collaboration, M. Ablikim *et. al.*, *Model-independent determination of the relative strong-phase difference between D^0 and $\bar{D}^0 \rightarrow K_{S,L}^0 \pi^+ \pi^-$ and its impact on the measurement of the CKM angle γ/ϕ_3* , *Phys. Rev. D* **101** (2020) 112002, [[2003.00091](#)].
- [31] **Belle** Collaboration, A. Poluektov *et. al.*, *Measurement of ϕ_3 with Dalitz plot analysis of $B^+ \rightarrow D^* K^{*+}$ decay*, *Phys. Rev. D* **73** (2006) 112009, [[hep-ex/0604054](#)].
- [32] J. Stern, H. Sazdjian, and N. H. Fuchs, *What $\pi\pi$ scattering tells us about chiral perturbation theory*, *Phys. Rev.* **D47** (1993) 3814–3838, [[hep-ph/9301244](#)].
- [33] J. Kambor, C. Wiesendanger, and D. Wyler, *Final state interactions and Khuri-Treiman equations in $\eta \rightarrow 3\pi$ decays*, *Nucl. Phys. B* **465** (1996) 215–266, [[hep-ph/9509374](#)].

- [34] G. Buchalla, A. J. Buras, and M. E. Lautenbacher, *Weak decays beyond leading logarithms*, *Rev. Mod. Phys.* **68** (1996) 1125–1144, [[hep-ph/9512380](#)].
- [35] L. Wolfenstein, *Parametrization of the Kobayashi-Maskawa Matrix*, *Phys. Rev. Lett.* **51** (1983) 1945.
- [36] **Particle Data Group** Collaboration, R. L. Workman *et. al.*, *Review of Particle Physics*, *PTEP* **2022** (2022) 083C01.
- [37] A. R. Edmonds, *Angular Momentum in Quantum Mechanics*. Princeton University Press, Princeton, New Jersey, 1957.
- [38] M. Matsuda, M. Nakagawa, K. Odaka, S. Ogawa, and M. Shin-Mura, *Comments on the D Meson Decays*, *Prog. Theor. Phys.* **59** (1978) 1396.
- [39] S. Kaptanoglu, *Nonleptonic Charm Decays*, *Phys. Rev. D* **18** (1978) 1554.
- [40] F. Niecknig, *Dispersive analysis of charmed meson decays*. PhD thesis, Bonn U., HISKP, 2016.
- [41] J. Kennedy and T. D. Spearman, *Singularities in partial-wave amplitudes for two ingoing and two outgoing particles*, *Phys. Rev.* **126** (May, 1962) 1596–1602.
- [42] N. L. Muskhelishvili, *Singular Integral Equations*. P. Noordhof, Groningen, 1953.
- [43] R. Omnès, *On the Solution of certain singular integral equations of quantum field theory*, *Nuovo Cim.* **8** (1958) 316–326.
- [44] A. Neveu and J. Scherk, *Final-state interaction and current algebra in $K_{3\pi}$ and $\eta_{3\pi}$ decays*, *Annals Phys.* **57** (1970) 39–64.
- [45] **FOCUS** Collaboration, J. M. Link *et. al.*, *Hadronic mass spectrum analysis of $D^+ \rightarrow K^- \pi^+ \mu^+ \nu$ decay and measurement of the $K^*(892)^0$ mass and width*, *Phys. Lett. B* **621** (2005) 72–80, [[hep-ex/0503043](#)].
- [46] **BaBar** Collaboration, P. del Amo Sanchez *et. al.*, *Analysis of the $D^+ \rightarrow K^- \pi^+ e^+ \nu_e$ decay channel*, *Phys. Rev. D* **83** (2011) 072001, [[1012.1810](#)].
- [47] **BESIII** Collaboration, M. Ablikim *et. al.*, *Study of $D^+ \rightarrow K^- \pi^+ e^+ \nu_e$* , *Phys. Rev. D* **94** (2016) 032001, [[1512.08627](#)].
- [48] **Belle** Collaboration, D. Epifanov *et. al.*, *Study of $\tau^- \rightarrow K_S \pi^- \nu_\tau$ decay at Belle*, *Phys. Lett. B* **654** (2007) 65–73, [[0706.2231](#)].
- [49] **BaBar** Collaboration, A. Adametz, *Studies of hadronic states containing kaons in τ decays at BaBar*, *Nucl. Phys. B Proc. Suppl.* **218** (2011) 134–139.

- [50] J. R. Pelaez and A. Rodas, *Pion-kaon scattering amplitude constrained with forward dispersion relations up to 1.6 GeV*, *Phys. Rev. D* **93** (2016) 074025, [[1602.08404](#)].
- [51] **KLF** Collaboration, M. Amarian *et. al.*, *Strange Hadron Spectroscopy with Secondary KL Beam in Hall D*, [2008.08215](#).
- [52] P. Estabrooks, R. K. Carnegie, A. D. Martin, W. M. Dunwoodie, T. A. Lasinski, and D. W. G. S. Leith, *Study of $K\pi$ Scattering Using the Reactions $K^\pm p \rightarrow K^\pm \pi^+ n$ and $K^\pm p \rightarrow K^\pm \pi^- \Delta^{++}$ at 13-GeV/c*, *Nucl. Phys. B* **133** (1978) 490–524.
- [53] D. Aston *et. al.*, *A Study of $K^- \pi^+$ Scattering in the Reaction $K^- p \rightarrow K^- \pi^+ n$ at 11-GeV/c*, *Nucl. Phys. B* **296** (1988) 493–526.
- [54] B. Moussallam, *Analyticity constraints on the strangeness changing vector current and applications to $\tau \rightarrow K \pi \nu_\tau$, $\tau \rightarrow K \pi \pi \nu_\tau$* , *Eur. Phys. J. C* **53** (2008) 401–412, [[0710.0548](#)].
- [55] B. Ananthanarayan, G. Colangelo, J. Gasser, and H. Leutwyler, *Roy equation analysis of $\pi\pi$ scattering*, *Phys. Rept.* **353** (2001) 207–279, [[hep-ph/0005297](#)].
- [56] B. Hyams, C. Jones, P. Weilhammer, W. Blum, H. Dietl, *et. al.*, *$\pi\pi$ Phase Shift Analysis from 600-MeV to 1900-MeV*, *Nucl. Phys. B* **64** (1973) 134–162.
- [57] M. Losty, V. Chaloupka, A. Ferrando, L. Montanet, E. Paul, *et. al.*, *A Study of $\pi^- \pi^-$ scattering from $\pi^- p$ interactions at 3.93-GeV/c*, *Nucl. Phys. B* **69** (1974) 185–204.
- [58] W. Hoogland, S. Peters, G. Grayer, B. Hyams, P. Weilhammer, *et. al.*, *Measurement and Analysis of the $\pi^+ \pi^+$ System Produced at Small Momentum Transfer in the Reaction $\pi^+ p \rightarrow \pi^+ \pi^+ n$ at 12.5-GeV*, *Nucl. Phys. B* **126** (1977) 109.
- [59] M. Jamin, J. A. Oller, and A. Pich, *S wave $K\pi$ scattering in chiral perturbation theory with resonances*, *Nucl. Phys. B* **587** (2000) 331–362, [[hep-ph/0006045](#)].
- [60] P. Büttiker, S. Descotes-Genon, and B. Moussallam, *A new analysis of πK scattering from Roy and Steiner type equations*, *Eur. Phys. J.* **C33** (2004) 409–432, [[hep-ph/0310283](#)].
- [61] O. Babelon, J. Basdevant, D. Caillerie, M. Gourdin, and G. Mennessier, *Meson Pair Production in Two-Photon Processes*, *Nucl. Phys. B* **114** (1976) 252.

- [62] J. F. Donoghue, J. Gasser, and H. Leutwyler, *The Decay of a Light Higgs Boson*, *Nucl. Phys. B* **343** (1990) 341–368.
- [63] **E791** Collaboration, E. M. Aitala *et. al.*, *Model independent measurement of S-wave $K^-\pi^+$ systems using $D^+ \rightarrow K\pi\pi$ decays from Fermilab E791*, *Phys. Rev. D* **73** (2006) 032004, [[hep-ex/0507099](#)]. [Erratum: *Phys. Rev. D* **74**, 059901 (2006)].
- [64] **FOCUS** Collaboration, J. M. Link *et. al.*, *The $K^-\pi^+$ S-wave from the $D^+ \rightarrow K^-\pi^+\pi^+$ decay*, *Phys. Lett. B* **681** (2009) 14–21, [[0905.4846](#)].
- [65] J. Gasser and A. Rusetsky, *Solving integral equations in $\eta \rightarrow 3\pi$* , *Eur. Phys. J. C* **78** (2018) 906, [[1809.06399](#)].
- [66] **BaBar** Collaboration, B. Aubert *et. al.*, *Improved measurement of the CKM angle γ in $B^\mp \rightarrow D^{(*)}K^{(\mp)}$ decays with a Dalitz plot analysis of D decays to $K_S^0\pi^+\pi^-$ and $K_S^0K^+K^-$* , *Phys. Rev. D* **78** (2008) 034023, [[0804.2089](#)].
- [67] A. Bondar and A. Poluektov, *On model-independent measurement of the angle ϕ_{13} using Dalitz plot analysis*, in *4th International Workshop on the CKM Unitarity Triangle (CKM 2006)*, 3, 2007. [[hep-ph/0703267](#)].
- [68] A. Bondar and A. Poluektov, *The Use of quantum-correlated D^0 decays for ϕ_3 measurement*, *Eur. Phys. J. C* **55** (2008) 51–56, [[0801.0840](#)].
- [69] **Belle** Collaboration, L. M. Zhang *et. al.*, *Measurement of $D^0 - \bar{D}^0$ Mixing Parameters in $D^0 \rightarrow K_S\pi^+\pi^-$ decays*, *Phys. Rev. Lett.* **99** (2007) 131803, [[0704.1000](#)].
- [70] J. P. Dedonder, R. Kaminski, L. Lesniak, and B. Loiseau, *Dalitz plot studies of $D^0 \rightarrow K_S^0\pi^+\pi^-$ decays in a factorization approach*, *Phys. Rev. D* **89** (2014) 094018, [[1403.2971](#)].
- [71] **CLEO** Collaboration, S. Kopp *et. al.*, *Dalitz analysis of the decay $D^0 \rightarrow K^-\pi^+\pi^0$* , *Phys. Rev. D* **63** (2001) 092001, [[hep-ex/0011065](#)].
- [72] **CLEO** Collaboration, N. Lowrey *et. al.*, *Analysis of the Decay $D^0 \rightarrow K_S^0\pi^0\pi^0$* , *Phys. Rev. D* **84** (2011) 092005, [[1106.3103](#)].
- [73] **CLEO** Collaboration, H. Muramatsu *et. al.*, *Dalitz analysis of $D^0 \rightarrow K_S^0\pi^+\pi^-$* , *Phys. Rev. Lett.* **89** (2002) 251802, [[hep-ex/0207067](#)]. [Erratum: *Phys. Rev. Lett.* **90**, 059901 (2003)].
- [74] **BaBar and Belle** Collaboration, I. Adachi *et. al.*, *Measurement of $\cos 2\beta$ in $B^0 \rightarrow D^{(*)}h^0$ with $D \rightarrow K_S^0\pi^+\pi^-$ decays by a combined time-dependent Dalitz plot analysis of BaBar and Belle data*, *Phys. Rev. D* **98** (2018) 112012, [[1804.06153](#)].

- [75] **MARK-III** Collaboration, J. Adler *et. al.*, *Resonant Substructure in $K\pi\pi$ Decays of Charmed D Mesons*, *Phys. Lett. B* **196** (1987) 107–112.
- [76] **E691** Collaboration, J. C. Anjos *et. al.*, *A Dalitz plot analysis of $D \rightarrow K\pi\pi$ decays*, *Phys. Rev. D* **48** (1993) 56–62.
- [77] **E687** Collaboration, P. L. Frabetti *et. al.*, *Analysis of three $D \rightarrow K\pi\pi$ Dalitz plots*, *Phys. Lett. B* **331** (1994) 217–226.
- [78] **LHCb** Collaboration, R. Aaij *et. al.*, *Measurement of the branching fractions of the decays $D^+ \rightarrow K^- K^+ K^+$, $D^+ \rightarrow \pi^- \pi^+ K^+$ and $D_s^+ \rightarrow \pi^- K^+ K^+$* , *JHEP* **03** (2019) 176, [[1810.03138](#)].
- [79] **BESIII** Collaboration, M. Ablikim *et. al.*, *Measurement of the branching fraction of the doubly Cabibbo-suppressed decay $D^0 \rightarrow K^+ \pi^- \pi^0$ and search for $D^0 \rightarrow K^+ \pi^- \pi^0 \pi^0$* , *Phys. Rev. D* **105** (2022) 112001, [[2203.01555](#)].
- [80] J. F. Donoghue, E. Golowich, and B. R. Holstein, *Dynamics of the Standard Model*. Cambridge University Press, 2nd ed., 2014.
- [81] M. Gronau, *Resonant two-body D decays*, *Phys. Rev. Lett.* **83** (1999) 4005–4008, [[hep-ph/9908237](#)].
- [82] M. Suzuki, *Partially Conserved Axial-Vector Current and the Nonleptonic K -Meson Decays*, *Phys. Rev.* **144** (1966) 1154–1157.
- [83] M. Bauer, B. Stech, and M. Wirbel, *Exclusive Nonleptonic Decays of D , D_s , and B Mesons*, *Z. Phys. C* **34** (1987) 103.
- [84] A. Anisovich and H. Leutwyler, *Dispersive analysis of the decay $\eta \rightarrow 3\pi$* , *Phys. Lett. B* **375** (1996) 335–342, [[hep-ph/9601237](#)].
- [85] J. M. Blatt and V. F. Weisskopf, *Theoretical nuclear physics*. Springer, New York, 1952.